HHS Public Access

Author manuscript

Cell Rep. Author manuscript; available in PMC 2023 September 15.

Published in final edited form as:

Cell Rep. 2023 July 25; 42(7): 112708. doi:10.1016/j.celrep.2023.112708.

Constitutively active autophagy dampens inflammation through metabolic and post-transcriptional regulation of macrophage cytokine production

Jinjin Xu[1,2], **Lingjia Kong**[1,2], **Blayne A. Oliver**[2], **Bihua Li**[1,2], **Elizabeth A. Creasey**[1,2], **Gaelen Guzman**[1], **Monica Schenone**[1], **Kimberly L. Carey**[1], **Steven A. Carr**[1], **Daniel B. Graham**[1,2], **Jacques Deguine**[1], **Ramnik J. Xavier**[1,2,3,*]

[1]Broad Institute of MIT and Harvard, Cambridge, MA 02142, USA

[2]Center for Computational and Integrative Biology, Department of Molecular Biology, Massachusetts General Hospital, Boston, MA 02114, USA

[3]Lead Contact

Summary

Autophagy is an essential cellular process that is deeply integrated with innate immune signaling; however, studies that examine the impact of autophagic modulation in the context of inflammatory conditions are lacking. Here, using mice with a constitutively active variant of the autophagy gene *Beclin1*, we show that increased autophagy dampens cytokine production during a model of macrophage activation syndrome and in adherent-invasive *Escherichia coli* (AIEC) infection. Moreover, loss of functional autophagy through conditional deletion of *Beclin1* in myeloid cells significantly enhances innate immunity in these contexts. We further analyzed primary macrophages from these animals with a combination of transcriptomics and proteomics to identify mechanistic targets downstream of autophagy. Our study reveals glutamine/glutathione metabolism and the RNF128/TBK1 axis as independent regulators of inflammation. Altogether, our work highlights increased autophagic flux as a potential approach to reduce inflammation and defines independent mechanistic cascades involved in this control.

Graphical Abstract

*Correspondence: xavier@molbio.mgh.harvard.edu.

Author Contributions

J.X., J.D., and R.J.X. designed the research. J.X. and B.O. performed experiments. J.X., L.K., and J.D. analyzed data. E.A.C. and B.L. contributed additional analytic tools for mouse and sequencing experiments. G.G., M.S., and S.A.C. performed and supervised proteomics experiments. J.X., K.L.C., D.B.G., J.D., and R.J.X. provided intellectual contributions throughout the project. J.X. and J.D. wrote the manuscript with contributions from all other authors. J.D. and R.J.X. supervised the project.

Declaration of Interests

R.J.X. is co-founder of Jnana Therapeutics and Celsius Therapeutics, Scientific Advisory Board member at Nestlé, and Board Director at MoonLake Immunotherapeutics; these organizations had no roles in this study. S.A.C. is a member of the scientific advisory boards of Kymera, PTM BioLabs, Seer and PrognomIQ; these organizations had no roles in this study.

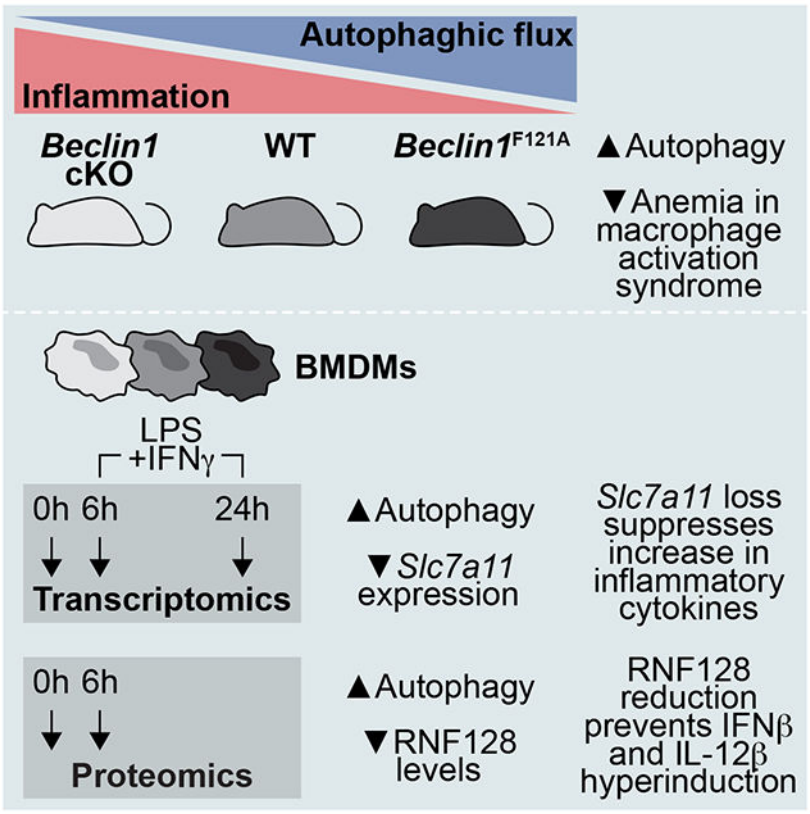

eTOC Blurb

Xu et al. describe independent transcriptional and post-transcriptional mechanisms in macrophages that underlie the regulation of inflammation by autophagy observed in models of infection and macrophage activation syndrome. They demonstrate that glutamine/glutathione metabolism and the RNF128/TBK1 axis function downstream of the core autophagy component Beclin1 to modulate proinflammatory cytokine production.

Introduction

Inflammation is an essential and evolutionarily conserved process that is initiated by innate immune cells in response to infection or tissue damage[1]; however, uncontrolled inflammation is a central element of many diseases and can contribute to further damage and impaired organ function[2]. The detection of pathogen- and/or damage-associated molecular patterns (PAMPs, DAMPs), mainly by macrophages and dendritic cells, rapidly leads to cytokine and chemokine release and additional immune infiltration, resulting in pathogen elimination and the initiation of tissue repair. This process requires tight regulation to prevent tissue damage and fibrosis. In addition to the direct regulation of signaling pathways associated with pattern recognition, inflammation is also modulated by the metabolic status of cells and tissues[3], in particular via multiple mechanisms of autophagy[4–6].

Multiple mouse models have demonstrated a systemic link between autophagy and inflammation. Mice lacking the autophagy gene *Epg5* and conditional knockout models

of *Atg14, Fip200, Atg5*, or *Atg7* in myeloid cells display elevated basal lung inflammation and influenza resistance[7]. Similarly, autophagy was shown to limit IFNγ production by myeloid cells derived from mice chronically infected with murine gammaherpesvirus 68 (MHV68), thus reducing systemic inflammation while fostering an environment that allows reactivation from latency[8]. Autophagic activity can both modulate apoptosis itself—via elimination of the damaged mitochondria that initiate apoptotic cascades—and the clearance of apoptotic corpses through the release of "find me" and "eat me" signals[9,10]. In addition, autophagy can modulate inflammatory signaling by regulating the inflammasome through several means[11–15]. First, autophagy inhibits IL-1β and IL-18 production through digestion of dysfunctional mitochondria, thereby preventing mitochondrial reactive oxygen species release that can activate the inflammasome. Second, autophagy is capable of targeting inflammasome complexes for degradation, which prevents cleavage of pro-IL-1β and pro-IL-18 into biologically active forms. Finally, autophagy machinery further regulates IL-1β levels by engulfing and degrading pro-IL-1β proteins.

Because of the multi-faceted effects of autophagy on cell states, the precise mechanisms and signaling pathways through which autophagy controls inflammation—and potential therapeutic opportunities that derive from this—have not been clearly delineated. Given its role in protein degradation, autophagy likely modulates both the transcriptional response to pattern recognition as well as the protein levels of sensors and effectors involved in inflammation. Therefore, a comprehensive view of transcriptomic, proteomic, and metabolic dynamics is necessary for understanding the underlying mechanism of autophagy-regulated inflammatory signaling.

To address this, we focused specifically on the core autophagy regulator Beclin1, initially discovered as a Bcl-2-interacting protein[16]. Suspected to function in autophagy due to its 24.4% amino acid sequence identity to the yeast autophagy protein Atg6, Beclin1 was indeed found to restore autophagic activity in *ATG6*-disrupted yeast and in autophagy-deficient breast cancer cells[17]. Beclin1 is part of the core endolysosomal phosphatidylinositol 3-kinase (PI3K-III) complexes I and II[18]. PI3K-III complex I is essential for the initiation of autophagy, while PI3K-III complex II functions in endosomal and autophagic maturation. The Levine and Heintz groups independently reported that homozygous deletion of *Beclin1* is embryonically lethal, and heterozygous deletion results in increased spontaneous tumorigenesis[19–21]. While germ-line knockout animals cannot be studied, conditional deletion of *Beclin1*[22] in myeloid cells implicated Beclin1 in protection against fatal disease due to cytokine storm syndromes[23]. Conditional deletion in endothelial compartments also leads to inflammation and an increase in endothelial permeability[24]. Critically, recent work revealed that an F121A point mutation in *Beclin1* knock-in mice significantly reduces the interaction of Beclin1 with its inhibitor Bcl-2, leading to constitutively active autophagy in multiple tissues[25] and increased healthspan and lifespan[26]. These mice also show improved insulin sensitivity and systemic activation of the energy regulator AMP-activated protein kinase (AMPK) through a mechanism of enhanced adiponectin secretion mediated by a Beclin1-exocyst interaction[27]. Thus, Beclin1-dependent models of deficient and hyperactive autophagy offer an ideal system to study the mechanisms by which autophagy regulates inflammation.

Here, we demonstrate that constitutively active autophagy curtails inflammation in multiple murine models, including a model of macrophage activation syndrome (MAS) and bacterial infection. We then focus on the mechanistic underpinnings of this regulation by evaluating bone-marrow-derived macrophages (BMDMs) derived from mice with deficient (*Beclin1*$^{flox/flox}$-LysM-Cre^{+}) or hyperactive (*Beclin1*$^{F121A/F121A}$) autophagy and the corresponding wild-type (WT) littermate control mice by whole proteome analysis and full-length RNA-sequencing. Our bidirectional analyses identify a large set of proinflammatory genes controlled by autophagy. Importantly, we also identify transporter genes regulated by Beclin1 and demonstrate that glutamine/glutathione metabolism may be an underlying mechanism for the regulation of inflammation by autophagy. Additionally, our proteomics analysis shows that Beclin1 can regulate innate immune signaling via the RNF128-TBK1 axis, with RNF128 protein levels being controlled by autophagy. Overall, our study demonstrates the potential of increased autophagic activity to control inflammation and provides direct mechanistic targets to leverage autophagy-dependent pathways implicated in cytokine regulation.

Results

Beclin1 F121A protects against MAS-like cytokine storm syndrome

We set out to examine whether the increased autophagic flux induced by the Beclin1 F121A mutation could prevent or limit hyperinflammation using MAS as a model. MAS is characterized by a cytokine storm, overwhelming inflammation, and multiorgan dysfunction. A murine model of repeated TLR9 stimulation with CpG DNA was found to replicate a MAS-like syndrome, displaying splenomegaly, hepatomegaly, cytopenias across multiple cellular compartments, hypercytokinemia, and hepatitis[28]. Disease induction is dependent on IL-12-induced IFNγ production, which correlates with activation of TLR9-responsive innate immune cells[29].

Following this MAS model[28], *Beclin1*$^{F121A/F121A}$ (hereafter, F121A) and WT littermate mice were repeatedly administered CpG DNA by intraperitoneal (ip) injection that resulted in peripheral pancytopenia (marked, for example, by a decrease in platelet and white blood cell counts), suggesting changes in immune cell differentiation and trafficking caused by repeated inflammatory stimulation (Figure S1A). However, when we looked specifically at anemia, a hallmark of MAS, we observed that CpG-treated F121A mice were partially protected compared to their WT littermates, as shown by higher hematocrit (HCT), hemoglobin (HGB) levels, and red blood cell (RBC) counts (Figure 1A). As anemia leads to a compensatory increase in erythropoiesis, we also examined erythrocyte differentiation in the spleen and bone marrow of CpG-treated mice (Figure 1B). Three erythroblast subsets are broadly separated by FSC and CD71 staining in Ter119^{+} cells: less mature EryA cells are FSC^{high}CD71^{+}, intermediate EryB progenitors are FSC^{low}CD71^{+}, and differentiated EryC cells are FSC^{low}CD71^{-}[30]. Consistent with less severe anemia, we observed a lower frequency and absolute number of EryA erythroblasts in the spleens of F121A mice compared to WT mice (Figure 1C). Similarly, the percentage of EryA erythroblasts in the bone marrow of F121A mice was decreased compared to WT mice (Figure S1B). We also observed a minor but statistically significant decrease in splenomegaly in CpG-treated

F121A mice with a corresponding decrease in splenic cellularity compared to their WT counterparts (Figure 1D). This decrease was associated with reduced numbers of B cells and innate immune cells, especially macrophages, in F121A compared to WT mice (Figure 1E, S1C).

To understand the immune regulation of this phenotype, we assessed the levels of cytokines found to be increased during MAS in both murine models and human patients[29,31–34]. Measuring serum levels of IL-12, IFNγ, TNF, and IL-6 on day 10 after CpG treatment, we observed an induction of IL-12 and IFNγ in WT mice that was suppressed in F121A mice (Figure 1F). In contrast, there were no significant differences in TNF and IL-6 induction between WT and F121A CpG-treated mice (Figure S1D). Together, our results show that constitutive autophagy partially protects from anemia observed in a CpG-induced MAS model, and that distinct levels of cytokines may play a role in this phenotypic difference.

To validate the impact of autophagy in this model, we next studied the effects of decreased autophagy following repeated CpG administration. For this, we used *Beclin1*$^{flox/flox}$-LysM-Cre^{+} (hereafter, cKO) mice to conditionally ablate *Beclin1* in myeloid cells. cKO and WT littermate control mice lacking Cre expression developed pancytopenia after CpG DNA injection (Figure S2A). CpG-treated cKO mice displayed more severe anemia than WT littermates (Figure S2B), with a higher frequency and absolute number of Ter119^{high} cells in the spleen 8 days after CpG administration (Figure S2C). We also observed more pronounced splenomegaly in CpG-treated cKO mice, which was associated with the increased number of Ter119^{high} cells , but no significant change in numbers of total splenocytes or specific populations (Figure S2D, E). We again assessed the levels of cytokines found to be increased during MAS in both murine models and human patients. Compared to serum from WT mice, serum from cKO mice showed higher amounts of IL-12 and IFNγ but no significant differences in TNF and IL-6 levels (Figure S2F). These results indicate that *Beclin1* cKO mice are more susceptible to CpG-induced MAS, and that this is associated with higher levels of at least some inflammatory mediators. Altogether, our findings suggest that modulating autophagic flux in either direction can influence inflammation and the resulting phenotypes in this model of MAS.

Beclin1 activity modulates intestinal inflammation in mice infected with AIEC

Given the central roles of autophagy and inflammation in responses to pathogens[35], we investigated whether the reduced inflammation observed in MAS in F121A mice was also seen in the context of infection and potentially associated with increased susceptibility to pathogens. To this end, we first infected F121A and WT littermates with adherent-invasive *E. coli* (AIEC), an Enterobacteriaceae commonly found in patients with Crohn's disease, a major form of inflammatory bowel disease (IBD)[36,37]. Autophagy was shown previously to restrict AIEC intracellular replication *in vitro*, as demonstrated by elevated bacterial numbers in infected ATG5-deficient mouse embryonic fibroblasts and ATG16L1 knockdown HeLa cells[38]. As AIEC is a human pathogen and not fully adapted to mice, we used the hypermotile AIEC strain NRG857c, which contains a mobile insertion sequence upstream of the master flagellar regulator, *flhDC*, that enhances AIEC invasion and establishment in the mucosal niche[39]. Interestingly, we did not observe any difference in bacterial burdens in

the stool of WT and F121A mice over the course of infection or in colonic tissue samples collected at days 2 and 8 (Figure S3A, B).

Next, we investigated whether inflammation was affected by Beclin1 activity in the context of a similar bacterial burden. We observed a lower frequency of macrophages in the colonic lamina propria of F121A mice than in WT mice, although the frequencies of other innate immune cells were not affected (Figure 2A). In addition, we cultured tissue explants for 24 hours to detect cytokine production and found that F121A colonic explants produced lower levels of IL-17A, IL-1β, IL-6, and TNF than WT colonic explants (Figure 2B). These findings indicate that the F121A mutant, resulting in higher autophagy levels, can limit the intestinal inflammatory response *in vivo*. Based on these results, we also evaluated the effect of decreased autophagy in macrophages during AIEC infection. For this, we infected cKO and littermate control mice with AIEC to monitor how decreased macrophage autophagy modulates bacterial burden and inflammation. Unlike the F121A mutation, deletion of *Beclin1* directly impacted bacterial burdens: at 2 days post infection, we observed a markedly lower bacterial burden in the colons of cKO mice relative to controls (Figure S3C). This reduced bacterial burden was nonetheless associated with a strong inflammatory response, including an increase of macrophages and neutrophils in the colonic lamina propria (Figure 2C) and an increase in IL-17A, IL-1β, IL-6, and TNF with a trend toward increased CXCL1 and CXCL2 in the supernatants of cKO colonic explants (Figure 2D, S3D). These observations suggest that modulating autophagic flux via either the deletion or deregulation of Beclin1 can also directly control the level of inflammation during enteric infection.

Beclin1 regulates cytokine and chemokine production in macrophages

To investigate a mechanistic basis for this regulation, we evaluated the responses of *Beclin1* cKO and F121A macrophages to stimulation with PAMPs. Given the role of autophagy in protein degradation, we examined both transcriptomic and proteomic responses at multiple timepoints to better understand how different modes of regulation contribute to inflammation control (Figure 3A). *Beclin1* cKO, F121A, and the respective WT control BMDMs were stimulated with LPS plus IFNγ for 0, 6, or 24 hours, then harvested for full-length RNA-sequencing (Methods, Figure S4A). A total of 31,994 genes (including both protein-coding and other transcripts) were detected in WT versus cKO RNA-sequencing and 29,381 in WT versus F121A RNA-sequencing, with 1,305 and 1,537 genes differentially expressed (FDR<0.05) between the respective comparisons (Figure S4B). Among these, only 313 genes were differentially expressed in both comparisons; most genes were not commonly modulated by *Beclin1* deletion and mutation and regulated post stimulation, suggesting that the influence of Beclin1 activity is highly dependent on context.

As a first approach, we performed a Gene Set Enrichment Analysis (GSEA) of *Beclin1* cKO and F121A transcriptomic changes between stimulated and baseline conditions (Methods). We focused on pathways that were differentially regulated in opposite directions in cKO and F121A transcriptomes since the former corresponds to decreased and the latter to increased autophagic flux. This approach revealed a set of KEGG and Reactome pathways that are regulated by autophagic activity across both genotypes (Methods, Table S1), including

vesicle trafficking, lysosomal signaling, and solute carrier (SLC) transporters (Figure 3B). Importantly, and consistent with our *in vivo* data, one of the top enriched pathways was innate immune signaling and included cytokines (*Il1a, Il1b, Il6, Il12a, Tnf*), chemokines (*Cxcl1, Cxcl2, Ccl3*), and type I interferon. After LPS+IFNγ stimulation, these genes were strongly downregulated in F121A compared to WT BMDMs but upregulated in Beclin1-deficient compared to WT BMDMs.

A time-course analysis of differentially expressed genes revealed a set with a similar pattern of opposing expression changes in cKO compared to F121A BMDMs (Figure 4A). These differences strengthened after LPS+IFNγ treatment, with an increased and decreased cytokine and chemokine response observed in cKO and F121A cells respectively.

Consistent with these observations, increases in cytokines (*Il1a, Il1b, Il6, Il12a, Il12b, Tnf*), chemokines (*Cxcl1, Cxcl2*), and type I interferon after LPS+IFNγ stimulation in *Beclin1* cKO BMDMs relative to WT BMDMs were confirmed by real-time quantitative PCR (qRT-PCR; Figure 4B–D) and protein detection (Figure 4E, F), indicating that deficient autophagy leads to hyperinflammation. Conversely, F121A BMDMs exhibited lower levels of the same inflammatory mediators (Figure 4B–F). Notably, IL-6, IL-12, TNF, and type I interferon demonstrated marked decreases at the protein level in F121A cells, while no significant differences in IL-1β were observed. Together, these results indicate that autophagy plays an important role in regulating inflammation and that modulation of Beclin1 in macrophages can either limit or enhance inflammatory cytokine production.

Beclin1 regulates inflammation through glutamine/glutathione metabolism

In addition to innate immune signaling genes, the integrated analysis of *Beclin1* cKO and F121A macrophage transcriptomics revealed opposing expression patterns in genes encoding SLC transporters, with higher expression in cKO BMDMs and lower expression in F121A BMDMs (Figure 3B, 5A). SLC transporters can modulate the intracellular levels of metabolites and ions, therefore representing an interesting family of candidates to test possible mechanisms of cytokine/chemokine regulation by Beclin1. First, we validated differences in SLC transporter expression by qRT-PCR (Figure 5B, S5A, S5B) and confirmed that the cystine/glutamate transport gene *Slc7a11* was strongly upregulated in stimulated cKO BMDMs and downregulated in stimulated F121A BMDMs. We also examined SLC7A11 protein expression in these cells and observed both a baseline increase of this transporter in cKO cells and a reduced induction in F121A cells, consistent with mRNA trends (Figure 5B).

As the metabolic demands of macrophages change during activation, we considered whether proinflammatory genes could be regulated by Beclin1 through glutamine metabolism. Glutamine is an amino acid that plays a key role in reducing inflammation and disease activity in animal models of colitis[40,41]. Previous studies have shown that glutamine deprivation impairs activation of M2 macrophages, and in contrast, leads to higher expression of M1-specific marker genes including *Il1a, Il1b, Il6, Il12a*, and *Tnf*[42]. First, we evaluated the effect of glutamine deprivation in WT macrophages stimulated with LPS+IFNγ for 24 hours. In agreement with previous studies, we observed increased transcription of proinflammatory cytokines and chemokines after glutamine deprivation

(Figure 5C). Glutamine deprivation also partially reverted expression differences of cytokines and chemokines between WT and *Beclin1* cKO (Figure 5D) and between WT and *Beclin1* F121A BMDMs (Figure 5E). Importantly, although not for all cytokines, this reversion towards WT expression levels occurred both in the case of high expression in cKO cells (with the expression difference of *Il1a, Il6, Tnf, Il12a*, and *Il12b* all lower without glutamine) and of low expression in F121A cells (with the expression difference of *Il1a*, *Il6*, *Tnf*, *Il12a*, *Il12b*, *Cxcl1*, and *Cxcl2* all higher without glutamine). Given the impact of extracellular glutamine addition, we directly measured levels of intracellular glutamine and downstream metabolites in *Beclin1* cKO and F121A BMDMs. Significantly lower glutamine levels were detected in cKO BMDMs compared to WT controls both with and without LPS+IFNγ stimulation, but no significant difference was observed between WT and F121A cells (Figure S5C, D). We observed a parallel increase in glutamate, glutathione (GSH), and glutathione disulfide (GSSG) in cKO BMDMs (Figure S5E, F). Because SLC7A11 imports components required for glutathione synthesis, we next evaluated whether deletion of *Slc7a11* could reduce the increased inflammatory cytokine production observed in cKO macrophages and indeed observed that all the inflammatory mediators tested except IL-1β and TNF were reduced (Figure 5F, S5G). The deletion of *Slc7a11* only had minor, and not statistically significant, effects on cytokine production in WT macrophages, likely reflecting the lower expression of these transporters in these cells. These data indicate that differences in glutamine availability or glutamine/glutathione metabolism may be an underlying mechanism for the regulation of inflammation by Beclin1, and that the transporter SLC7A11 plays a key role in mediating these effects.

The effects of Beclin1 deficiency on gene expression have low concordance in proteomics

Given the protein level differences observed in *Beclin1* cKO macrophages, we focused on this genotype and performed a full proteomic analysis using TMT10 on cKO and WT control BMDMs with and without a 6-hour LPS+IFNγ treatment (Methods, Figure S6A). At baseline and after stimulation respectively, 441 proteins and 493 proteins were differentially expressed, with 239 proteins in common (Figure S6B).

A total of 4,752 genes/proteins were measured from both proteomics (4,752/5,096) and transcriptomics (4,752/31,994) of WT and *Beclin1* cKO BMDMs (Figure 6A). We used these common genes/proteins to study relationships between WT and cKO BMDM transcriptomes and proteomes (Methods), revealing 4 categories: concordant (consistent change in abundance at transcript and protein levels), discordant (opposite change in abundance at transcript and protein levels), mixed (only significant difference at either transcript or protein level), or unchanged (no significant difference at either transcript or protein level). Many concordant genes/proteins were observed in both WT and cKO BMDMs in response to LPS+IFNγ treatment (Figure 6B, upper panels). This concordance was lower across genotypes, i.e. when comparing WT or cKO BMDMs regardless of treatment (Figure 6B, lower panels). Although the assessment of this concordance is complicated by the different sensitivities of the two technologies, the difference likely reflects the fact that stimulation produces acute changes in transcripts that rapidly translate into proteins, whereas underlying genotypic, and therefore autophagic, differences lead to a complex regulatory network that can uncouple mRNA and protein levels. To directly

evaluate the role of sensitivity in these correlations, we sorted them across gene abundance. Comparing baseline versus stimulation, there was a clear link between gene/protein concordance and correlation (Spearman's $\rho>0.6$ for genes in the 4th quartile of abundance) (Figure 6C). However, this was not the case when comparing across genotypes, which reinforces the idea that differences in concordance reflect true regulation and not solely a discrepancy in sensitivity of the mRNA and protein data acquisition. Based on these observations and the role of Beclin1 in modulating autophagy (and thus potentially protein degradation), we opted to focus additional efforts on changes detected by proteomics alone, as these may represent additional modes of post-transcriptional regulation that differ from the glutamine-dependent regulation described by transcriptomics.

Beclin1 regulates inflammatory mediators in an RNF128/TBK1-dependent manner

Analyzing proteins detected as differentially abundant only by proteomics and not transcriptomics (Table S2), we identified 93 proteins that were increased in *Beclin1* cKO BMDMs and 97 proteins that were markedly decreased in the absence of Beclin1. As a validation of our system, proteins that are directly implicated in the formation of autophagosomes, such as autophagy cargo receptors p62 and TAX1BP1, were increased in *Beclin1* cKO BMDMs where they are no longer being degraded through autophagic flux. Besides multiple metabolic pathways (metabolism of glutathione, nucleotides, amino acids and derivatives), the analysis of these differentially abundant proteins revealed multiple genes involved in innate immunity and antigen processing cross presentation (Table S2). Among these, we decided to focus particularly on innate immune signaling and observed an enrichment of RNF128 in *Beclin1* cKO cells. RNF128 is an E3 ubiquitin ligase that can positively modulate IFN-β signaling through K63-linked polyubiquitination and activation of TBK1[43]. Notably, TBK1 is also a well-recognized link between autophagy and inflammation, as TBK1 and IKKε function as non-canonical IκB kinases downstream of Toll-like receptors (TLRs), Rig1-like receptors, DDX3X, and DNA receptors[44]. TBK1 can also directly phosphorylate the autophagy cargo receptors optineurin and p62[45]. Moreover, previous reports showed that inhibition of autophagy dysregulates TBK1 signaling[46,47]. Therefore, we hypothesized that Beclin1 may degrade RNF128 to regulate TBK1 activation and proinflammatory mediators.

To test this hypothesis and to validate whether the mechanisms identified in Beclin1-deficient macrophages are also at play in the context of constitutively active autophagy, we first measured RNF128 protein expression and TBK1 activation (marked by phosphorylation) in cKO, F121A, and respective WT control BMDMs after LPS+IFNγ stimulation for 0, 6, or 24 hours (Figure 7A, B). As expected, p62 levels were increased in cKO and decreased in F121A BMDMs compared to WT controls, indicating that autophagic flux is modulated in these conditions. Beclin1-deficient BMDMs exhibited higher levels of RNF128 and phosphorylated TBK1 (p-TBK1) compared to WT BMDMs, while F121A cells displayed decreased RNF128 and p-TBK1 levels. Confirming previous observations on the role of RNF128 in TBK1 signaling[43], we tested K63-linked ubiquitination of TBK1 and indeed observed a decreased ubiquitination in F121A cells compared to WT cells (Figure S7A). To further understand the impact of these changes on innate immune signaling, we assessed NFkB activation by measuring phosphorylated p65 in WT, cKO, and F121A

cells. Consistent with increased TBK1 activity, we found increased levels of phosphorylated NF-κB p65 in cKO BMDMs and decreased levels in F121A BMDMs compared to the corresponding WT controls (Figure S7B). Altogether, these results suggest a model where autophagy modulates RNF128 levels, which in turn regulate TBK1 ubiquitination, activity, and ultimately downstream innate immune signaling.

We then confirmed that decreased RNF128 levels were directly linked to lysosomal degradation by treating WT BMDMs with the lysosomal inhibitor bafilomycin A1 (BafA1). BMDMs showed a significant accumulation of RNF128 after lysosomal inhibition, similar to observed levels of p62 and LC3, which are known to be degraded via this pathway (Figure 7C). As expected, BafA1 treatment eliminated the difference in RNF128 levels between cKO and WT BMDMs and restored the decreased RNF128 protein level observed in F121A cells, again similar to LC3 and p62 (Figure 7D, E). Taken together, these results strongly suggest that protein levels of RNF128 are modulated by autophagy and specifically the lysosomal degradation pathway.

To evaluate the degree to which the cytokine differences we observed are related to the RNF128/TBK1 axis, we performed a knockout of *Rnf128* in *Beclin1* cKO and WT BMDMs (Figure 7F, S7C). Deletion of *Rnf128* reverted the increases in *Il12b* and *Ifnb* transcription observed with *Beclin1* knockout but did not reduce *Il1b* and *Il6* levels. These data suggest that the RNF128 E3 ligase is a key regulator of IL-12β and IFNβ induction in the context of decreased autophagy; however, additional mechanisms of regulation for other cytokines may exist. We confirmed that these effects were linked to TBK1 by comparing our results to those obtained with a TBK1/IKKε inhibitor. The inhibitor MRT67307 strongly reduced *Ifnb, Il12a*, and *Il12b* expression and rescued the changes owing to Beclin1 deficiency or activation (Figure S7D, E). In contrast, MRT67307 did not restrict the expression of other cytokines (*Il1a, Il1b, Il6*) and could even induce their levels further. Together, these results suggest that Beclin1 regulates type I interferon and the proinflammatory cytokine IL-12 in an RNF128/TBK1-dependent manner, specifically with autophagy affecting the degradation of RNF128 that in turns modulates TBK1 activity and its impact on downstream immune signaling.

Discussion

While the impact of autophagy on inflammation is well appreciated, regulation could occur through a variety of cell types and mechanisms, including transcriptional and post-transcriptional changes as well as the handling of cargo such as apoptotic cells. Additionally, while many studies have demonstrated the occurrence of inflammatory disorders in autophagy-deficient models, whether increasing autophagy is a viable strategy to prevent or limit inflammation remains unclear.

Our studies of *Beclin1*$^{F121A/F121A}$ knock-in mice demonstrate that this mutation limits cytokine production and inflammation in both a MAS-like model and an infection setting. Interestingly, reduced inflammation during infection was not associated with impaired pathogen clearance, although it will be important to confirm this using pathogens with higher virulence given that AIEC, including the hypermotile strain used here, is not fully

adapted to murine hosts. Nevertheless, our results suggest that increasing autophagic activity may be beneficial during acute inflammation and reinforce previous studies showing that the F121A mutation improves healthspan[26]. As we uncovered macrophage-specific roles through our *in vitro* systems, it is tempting to speculate that the immune compartment could directly contribute to increased healthspan by decreasing aging-associated inflammation, termed inflammaging[48]. Testing this hypothesis will require future studies using bone marrow chimeras or cell-specific expression of the F121A mutant.

Beyond examining the effects on inflammation of enhancing autophagic activity, we also aimed to identify specific mechanistic pathways downstream of Beclin1 that could expose previously unknown targets of regulation. By using a combination of transcriptomics and proteomics, we were able to reveal two independent and complementary pathways: one relying on transcriptional regulation of transporters that affects glutamine/glutathione metabolism and one relying on degradation of RNF128, a regulator of innate signaling pathways via TBK1. Importantly, our transcriptomic analysis revealed that *Rnf128* was not regulated at the mRNA level, thus requiring a proteomic approach for identification. Our results are consistent with a report demonstrating that ATG16L1-deficient macrophages (either uninfected or in the context of *Shigella flexneri* infection) have increased levels of RNF128[49], suggesting that RNF128-mediated hyperinflammation may be a general feature of decreased autophagy. Importantly, glutamine/glutathione metabolism and RNF128 modulated cytokine induction in distinct ways, with RNF128 controlling IL-12 and type I interferon but not other proinflammatory cytokines. Additional pathways are likely involved in the regulation of inflammation by autophagy. At a minimum, previous work and this study have shown that autophagy regulates inflammation through cargo elimination, signaling pathways, and cell state and metabolism. Metabolism and mTOR activity are also key regulators of autophagy, demonstrating the close connection between these processes. We performed our studies with LPS+IFNγ-treated, M1-like cells, which switch their metabolism towards glycolysis during activation[50]. The link between glutamine and autophagy we observed may therefore exert distinct regulatory effects in cells that rely primarily on oxidative phosphorylation instead of glycolysis, and it will be important to understand how autophagy influences macrophage function in distinct metabolic settings.

Several roles for TBK1 at different stages of autophagy have been described. TBK1 regulates autophagy initiation by phosphorylating Syntaxin17, which in turn controls formation of the $ATG13^{+}FIP200^{+}$ mammalian pre-autophagosomal structure (mPAS)[51]. TBK1 is also required for autophagosome maturation involving the assembly of PI3K-III complex II[52] and promotes autophagy-mediated antimicrobial defense. Multiple Beclin1-containing complexes act throughout the autophagy process[18]. The core Beclin1-VPS34-VPS15 complex interacts with ATG14L to function in autophagy initiation, and the same complex associates with UVRAG to modulate autophagosome maturation. The binding of Rubicon to the Beclin1 core complex though UVRAG neutralizes the ability of Rubicon to sequester Rab proteins and inhibit autophagosome maturation. Here, we show that Beclin1 regulates RNF128-TBK1 signaling via the lysosomal degradation pathway in proinflammatory macrophages, but the precise molecular mechanisms at play during

inflammation—including which Beclin1 complex coordinates with RNF128-TBK1 and how—require further characterization.

We revealed the effect of Beclin1 on cytokine production downstream of TLR signaling during inflammation and infection; however, direct modulation of TLRs by an autophagy protein may also play a role. For example, a study in skeletal muscle showed a direct association between TLR9 and Beclin1 that activates AMPK and glucose metabolism during exercise[53]. This interaction was enhanced by energy stress and inhibited by a mutation in Bcl-2 that stabilizes its binding with Beclin1. TLR9 is additionally involved in the assembly of PI3K-III complex II, which comprises Beclin1, UVRAG, and the vacuolar sorting proteins VPS34 and VPS15[18]. Further work is required to investigate the different layers of crosstalk between TLRs and Beclin1 during inflammation and infection.

In summary, our work reinforces the role of autophagy as a modulator of inflammation and indicates that this effect is mediated by distinct mechanisms functioning during different stages of innate immune activation. Our findings provide a rationale for targeting autophagy therapeutically, potentially in both acute and chronic inflammatory conditions, and importantly identify potential targets with specific effects on cytokine production.

Limitations of the study

Our *in vivo* analyses of the Beclin1 F121A mutation focused on global knock-in mice; conditional strains will be critical to understand how autophagy can modulate inflammation and healthspan through different cell types. We also note that Beclin1 controls both canonical and non-canonical autophagy pathways, therefore additional genetic models will be required to further dissect the impact of distinct autophagic mechanisms on inflammation. From a therapeutic standpoint, the impact of autophagy induction will need to be evaluated in additional and potentially more severe disease models, as the MAS model used here is generally considered to replicate a mild form of the syndrome. Finally, while we describe two potential mechanisms of control of inflammation by autophagy, we note that not all cytokines were equally affected by these pathways and that some aspects of the phenotypes we observed, such as changes in glutamine levels, were restricted to cKO cells and may be compensated by metabolic feedback in F121A cells. Cytokines that were not sensitive to perturbations of these two pathways may be regulated through other epigenetic, metabolic, or signaling modalities. A more complete understanding of these mechanisms will likely require further investigations that can leverage the proteogenomic data presented here.

STAR Methods

RESOURCE AVAILABILITY

Lead Contact—Further information and requests for resources and reagents should be directed to and will be fulfilled by the lead contact, Ramnik J. Xavier (xavier@molbio.mgh.harvard.edu).

Materials Availability—This study did not generate new unique reagents.

Data and Code Availability

- RNA-sequencing data have been deposited at GEO and are publicly available as of the date of publication under accession number GSE206124. Proteomic data have been deposited at MassIVE and are publicly available as of the date of publication under accession number MSV000092110. Accession numbers are additionally listed in the Key Resources Table.
- This paper does not report original code.
- Any additional information required to reanalyze the data reported in this paper is available from the Lead Contact upon request.

EXPERIMENTAL MODEL AND SUBJECT DETAILS

Mice—All mouse experiments complied with relevant ethical regulations and were performed according to protocol number 2003N00158 approved by the Institutional Animal Care and Use Committee (IACUC) at the Massachusetts General Hospital. *Beclin1*$^{flox/flox}$-LysM-Cre^{+} and *Beclin1*$^{flox/flox}$-LysM-Cre^{-} mice were provided by the Virgin lab (Washington University in St. Louis)[8], and *Beclin1*$^{F121A/F121A}$ mice were provided by the Levine lab (University of Texas Southwestern)[26]; these mice were generated on the C57BL/6 background. All mice were maintained in specific pathogen-free conditions and co-housed in the same room at the Massachusetts General Hospital's animal facility maintained on a 12 hour light:dark cycle with a room temperature of 21°C and relative humidity of 30-70%. *Beclin1*$^{flox/flox}$-LysM-Cre^{-} mice were littermates of *Beclin1*$^{flox/flox}$-LysM-Cre^{+} mice. WT mice were littermates of *Beclin1*$^{F121A/F121A}$ mice. All mouse experiments were performed using male and female mice aged 8-12 weeks. Mice were age- and sex-matched in each experiment. The number of mice used in each experiment is provided in the figure legends.

Bone marrow-derived macrophages—Bone marrow from *Beclin1*$^{flox/flox}$-LysM-Cre^{+} and *Beclin1*$^{flox/flox}$-LysM-Cre^{-} mice or *Beclin1*$^{F121A/F121A}$ and littermate control mice were cultured in DMEM supplemented with 10% fetal bovine serum, 100U/ml penicillin, 100mg/ml streptomycin, and 20ng/mL murine M-CSF (PeproTech) for 7 days to generate BMDMs. On day 7, adherent BMDMs were dissociated from the plate and re-plated for experiments. BMDMs were stimulated with 100ng/ml LPS (Sigma-Aldrich) plus 100ng/ml IFNγ (BD Biosciences) for M1 activation for the indicated duration. For the glutamine deprivation assay, media containing glutamine was removed, and cells were washed twice with warm PBS, then cultured in media without glutamine overnight before stimulation.

Generation of knockout BMDMs by CRISPR-Cas9—Alt-R CRISPR–Cas9 System (IDT): Bone marrow was harvested from *Beclin1*$^{flox/flox}$-LysM-Cre^{+} and *Beclin1*$^{flox/flox}$-LysM-Cre^{-} mice and washed twice in PBS, pelleted, and ribonucleoprotein (RNP) complexes (crRNA–tracrRNA–Cas9) and P3 Primary Cell buffer were added before transfer to nucleofection chambers. The complexes were delivered by electroporation using CM137 pulse on an Amaxa 4D-Nucleofector (Lonza). Electroporated cells were recovered in pre-warmed cell culture medium for 120 minutes at 37 °C before growth in the BMDM

differentiation condition. Knockout/knockdown was confirmed by western blot or Sanger sequencing.

CpG-induced MAS-like syndrome—Mice were given intraperitoneal (ip) injections on days 0, 2, 4, 7 and 9 with PBS or CpG1826 (50μg) (INVIVOGEN Cat# tlrl-1826) following an established MAS model[28]. On day 8 or day 10, whole blood was collected for a complete blood count analysis. On day 10 mice were euthanized, and blood, spleen, and bone marrow were taken for cytokine measurement, erythroid progenitor analysis, and immunophenotyping. Spleen and bone marrow cells were prepared as previously described[30]. Cells were counted using a hemocytometer, and 1-2 million cells/200μl per sample were taken for flow cytometry analysis. Cells were washed with PBS and incubated with live/dead fixable Zombie UV dye (BioLegend Cat# 423108) in PBS at room temperature for 15 minutes. Cells were stained with fluorescent-conjugated antibodies and Biotin-conjugated antibodies on ice for 1 hour. APC Streptavidin (BioLegend Cat# 405207) staining on ice for 1 hour was used for detecting Biotin-conjugated antibodies. For analysis of erythroid progenitors, cells were stained with antibodies against Biotin-CD3 (BioLegend Cat# 100303, RRID:AB_312668), Biotin-B220 (BioLegend Cat# 103204, RRID:AB_312989), Biotin-CD11b (BioLegend Cat# 101204, RRID:AB_312787), Biotin-Gr-1 (BioLegend Cat# 108404, RRID:AB_313369), Biotin-F4/80 (BioLegend Cat# 123106, RRID:AB_893501), Biotin-CD11c (BioLegend Cat# 117304, RRID:AB_313773), Biotin-NK1.1 (BioLegend Cat# 108703, RRID:AB_313390), CD71 (BioLegend Cat# 113812, RRID:AB_2203382), and Ter119 (BioLegend Cat# 116234, RRID:AB_2562917). For immunophenotyping, cells were stained with antibodies against CD19 (BioLegend Cat# 115521, RRID:AB_389307), CD11b (BioLegend Cat# 101243, RRID:AB_2561373), F4/80 (BioLegend Cat# 123117, RRID:AB_893489), Ly6G (BioLegend Cat# 127610, RRID:AB_312989), CD11c (BioLegend Cat# 117339, RRID:AB_2562414), CD3e (BD Biosciences Cat# 563565, RRID:AB_2738278), CD8a (BioLegend Cat# 100752, RRID:AB_2563057), CD4 (BD Biosciences Cat# 553653, RRID:AB_394973), CD45 (BD Biosciences Cat# 103128, RRID:AB_493715), and MHCII (BioLegend Cat# 107639, RRID:AB_2565894). Stained cells were fixed with 2% paraformaldehyde (PFA) at room temperature for 10 minutes. Samples were analyzed using Cyteck Aurora flow cytometer and FlowJo software.

Adherent-invasive *E. coli* (AIEC) infection—The hypermotile AIEC strain NRG857c was provided by Dr. Brian K. Coombes[39]. AIEC were cultured in LB broth containing chloramphenicol (34 μg/mL) and carbenicillin (50 μg/mL) at 37°C with shaking overnight (~16 hours), followed by subculture for 4 hours and OD600 measurement to calculate counts before infecting mice. Mice were administered 20mg streptomycin via oral gavage 24 hours prior to infection with $2x10^9$ colony-forming units (CFUs) of AIEC. Infection progress was monitored daily by plating serial dilutions from fresh stool homogenates on LB agar plates. At the indicated days post infection, mice were euthanized and tissues were harvested for analysis. Mid-colon tissue samples were homogenized and plated on LB agar plates for CFU counts. For immunophenotyping of the intestine, the intestine was opened and cleaned in room temperature 1X PBS, cut into small pieces, and incubated with pre-warmed epithelial strip buffer (5% FBS, 5mM EDTA, 1mM DTT, 15mM HEPES, 1X HBSS) spinning at

1,600rpm at 37°C for 30 minutes. Tissues were washed at least twice with wash media (1% FBS, 15mM HEPES, 1X HBSS) to remove EDTA prior to digestion with Liberase TL (150ug/ml, Roche, Cat# 05401020001) containing 0.1mg/ml DNase spinning at 1,600rpm at 37°C for 30 minutes. Cold stop buffer (5% FBS, 1mM EDTA, 1X HBSS) was added, and the tissues were placed on ice to stop the reaction. Single cells were obtained by passage through a 100μM nylon filter. Lamina propria cells were obtained using Percoll gradient centrifugation. Lamina propria cells were stained with fluorescent-conjugated antibodies against CD45 (BioLegend Cat# 103128, RRID:AB_493715), MHCII (BioLegend Cat# 107620, RRID:AB_493527), F4/80 (BioLegend Cat# 123120, RRID:AB_893479), CD64 (BioLegend Cat# 139306, RRID:AB_11219391), CD11c (BioLegend Cat# 117318, RRID:AB_493568), CD11b (BioLegend Cat# 101262, RRID:AB_2572122), siglecF (BD Biosciences Cat# 562757, RRID:AB_2687994), and Ly6G (BioLegend Cat# 127633, RRID:AB_2562937). Samples were analyzed using Cyteck Aurora flow cytometer and FlowJo software.

METHOD DETAILS

RNA-sequencing—BMDMs were generated as described above, where 3 mice per genotype (*Beclin1*$^{flox/flox}$-LysM-Cre^{+} and *Beclin1*$^{flox/flox}$-LysM-Cre^{-}) or 2 mice per genotype (*Beclin1*$^{F121A/F121A}$ and WT littermate controls) were considered biological replicates, and 3 technical replicates were performed for each biological replicate. After stimulation with LPS+IFNγ for the indicated time (0, 6, or 24 hours), BMDMs were harvested and lysed in RLT buffer (Qiagen). Libraries were constructed from lysates using the Smart-Seq2 protocol. Briefly, RNA was reverse transcribed with an oligo(DT) primer and template switch oligo, and the resulting cDNA was preamplified and used for tagmentation (Nextera XT) and barcoding. Libraries were sequenced with a 75 cycle NextSeq kit and the following parameters: paired End: Index1 8, Index2 8, Read1 38, Read2 38.

Sample preparation for proteomic analysis—BMDMs from 3 pairs of mice (*Beclin1*$^{flox/flox}$-LysM-Cre^{+} and *Beclin1*$^{flox/flox}$-LysM-Cre^{-}) were generated as described above. BMDMs for the same genotype were combined and stimulated with LPS+IFNγ for 6 hours or left unstimulated (0h). Two technical replicates were performed for the 0-hour stimulation, and 3 technical replicates were performed for the 6-hour stimulation. After stimulation, BMDMs were harvested and sent to the Broad Institute of MIT and Harvard for proteomic measurement and analysis.

Protein digestion, labeling, and fractionation—Cells were centrifuged, pellets were lysed in 8M urea, and protein levels were quantified by BCA before an overnight LysC/trypsin tryptic digest. The supernatants were then reduced (2 μL 500 mM dithiothreitol for 30 minutes at room temperature) and alkylated (4 μL 500 mM iodoacetic acid for 45 minutes in the dark), and a long overnight digestion was performed with 2 μg (4 μL) trypsin. The reactions were then quenched with 20 μL 10% formic acid and desalted on 1cc 10 mg Oasis HLB cartridges.

Desalted peptides were labeled with TMT10 reagents (Thermo Fisher Scientific, lot# RF231770) according to the manufacturer's instructions. Peptides were resuspended in 25 μL of fresh 100mM HEPES buffer. The labeling reagent was resuspended in 42 μl of acetonitrile, and 10 μl was added to each sample as described in Table S3.

After a 1-hour incubation, the reaction was quenched with 8μl of 5% hydroxylamine. Differentially labeled peptides were subsequently pooled (100μg each channel) and fractionated by offline BRP chromatography and finally concatenated to 24 fractions.

Protein identification with nanoLC–MS system—Reconstituted peptides were separated on an online nanoflow EASY-nLC 1000 UHPLC system (Thermo Fisher Scientific) and analyzed on a benchtop Orbitrap Q Exactive plus mass spectrometer (Thermo Fisher Scientific). The peptide samples were injected onto a capillary column (Picofrit with 10 μm tip opening / 75 μm diameter, New Objective, PF360-75-10-N-5) packed in-house with 20 cm C18 silica material (1.9 μm ReproSil-Pur C18-AQ medium, Dr. Maisch GmbH, r119.aq). The UHPLC setup was connected with a custom-fit microadapting tee (360 μm, IDEX Health & Science, UH-753), and capillary columns were heated to 50°C in column heater sleeves (Phoenix-ST) to reduce backpressure during UHPLC separation. Injected peptides were separated at a flow rate of 200 nL/min with a linear 50 min gradient from 100% solvent A (3% acetonitrile, 0.1% formic acid) to 30% solvent B (90% acetonitrile, 0.1% formic acid), followed by a linear 9 min gradient from 30% solvent B to 60% solvent B and a 1 min ramp to 90% B. The Q Exactive instrument was operated in the data-dependent mode acquiring HCD MS/MS scans (R=17,500) after each MS1 scan (R=70,000) on the 12 top most abundant ions using an MS1 ion target of $3x10^6$ ions and an MS2 target of $5x10^4$ ions. The maximum ion time utilized for the MS/MS scans was 120 ms; the HCD-normalized collision energy was set to 28; the dynamic exclusion time was set to 20s, and the peptide match and isotope exclusion functions were enabled.

Real-time quantitative PCR (qRT-PCR)—RNA was extracted from BMDMs using RNeasy (Qiagen) following the manufacturer's protocol. RNA was reverse-transcribed to cDNA using iScript Synthesis kit (Bio-Rad). For quantitative RT-PCR analysis, the cDNA was subjected to RT-PCR using SYBR Green Supermix (Bio-Rad) on a CFX Opus 384 Real-Time PCR system (Bio-Rad). Each experiment included 2-4 biological replicates and was repeated 2-3 times. Relative mRNA abundance was calculated by the ΔΔCt method with samples normalized to WT control and actin. qRT-PCR primer sequences are provided in Table S4.

Cytometric bead array—Samples were collected from BMDM culture supernatants, colons that were cultured for 24 hour *ex vivo* after isolation from mice, or serum isolated from mouse blood to measure cytokines production using the Cytometric Bead Assay Flex Set (BD Biosciences) following the manufacturer's protocol.

Western blot—BMDMs were generated as described above, then stimulated as described in the figure legends. After stimulation, BMDMs were harvested and lysed with NP40 lysis buffer (50 mM Tris-HCl, 150 mM NaCl, 5 mM EDTA, 1% NP-40, 5% glycerol, protease inhibitors) for 30 minutes on ice, then centrifuged for 15 minutes

at 12,000rpm at 4°C. The supernatant was collected and added to SDS sample buffer and resolved in a 4-12% gradient SDS gel (Bio-Rad). Separated proteins were transferred to PVDF membrane and immunoblotted with primary antibodies. Blots were then incubated with horseradish peroxidase (HRP) secondary antibodies and visualized by chemiluminescence. Antibodies used were: anti-RNF128 (Abcam Cat# ab137088), anti-TBK1 (Cell Signaling Technology Cat# 3504, RRID:AB_2255663), anti-phospho-TBK1 (Ser172) (Cell Signaling Technology Cat# 5483, RRID:AB_10693472), anti-NF-κB p65 (Cell Signaling Technology Cat##8242,RRID:AB_10859369), anti-Phospho-NF-κB p65 (Ser536) (Cell Signaling Technology Cat#3033), anti-LC3 (Cell Signaling Technology Cat# 2775, RRID:AB_915950), anti-p62 (APR American Research Products Cat# 03-GP62-C, RRID:AB_1542690), anti-GAPDH (Cell Signaling Technology, Cat# 2118, RRID:AB_561053), anti-actin (Sigma-Aldrich Cat# A1978, RRID:AB_476692), anti-SLC7A11 (Cell Signaling Technology Cat#98051,RRID:AB_2800296), anti-K63-linkage Specific Polyubiquitin (Cell Signaling Technology Cat#5621,RRID:AB_AB_10827985), goat anti-rabbit HRP secondary antibody (Agilent Cat# P0448, RRID:AB_2617138), goat anti-mouse HRP secondary antibody (Agilent Cat# P0447, RRID:AB_2617137), and rabbit anti-guinea pig HRP-conjugated antibody (Dako Cat# P-0141).

Glutamine, Glutamate, and Glutathione Assays—1 million BMDMs were harvested and lysed in indicated buffers on ice for 15 minutes. Samples were centrifuged at top speed for 5 minutes at 4°C using a microcentrifuge to remove any insoluble material. Supernatants were collected and used for the following assays according to the manufacturer's protocols: glutamine assay kit (Abcam,Cat# ab197011), glutamate assay kit (Abcam,Cat#ab83389), and glutathione assay kit (Thermo Fisher Scientific,Cat# EIAGSHC, used to measure both glutathione and glutathione disulfide).

QUANTIFICATION AND STATISTICAL ANALYSIS

Statistical analysis—Statistical analysis was done using Prism (GraphPad Software) or Excel (Microsoft Office). Data represent the mean with standard error of the mean (SEM). Two-tailed unpaired t-test, multiple unpaired t-test, or one-way ANOVA Šídák's multiple comparisons test were used for statistical analysis. The statistical details of the experiments can be found in the figure legends. *$p<0.05$; **$p<0.01$; ***$p<0.001$, ****$p<0.0001$. $p\geq0.05$ was considered not significant (ns). No statistical methods were used to pre-determine sample sizes, but our sample sizes provided sufficient power for statistical analysis. The sample size (n) reported in each figure legend refers to biological replicates unless otherwise indicated in the Methods. No data were excluded from the analyses. Age- and sex-matched mice were allocated into experimental groups based on genotype. Mice were randomly assigned to treatment groups where applicable. Data collection and analysis were performed in a blinded manner whenever possible. Data analysis was not blinded for experiments grouped by genotype due to the experimental design, but unbiased quantification was applied to obtain the results.

Transcriptomics data analysis—Sequencing reads were aligned to the mouse reference genome mm10 using Tophat2[54]. Read counts for each gene were then summarized by Htseq-count[55]. The R/Bioconductor package edgeR[56] was used to identify differentially

expressed (DE) genes. Genes with a false discovery rate (FDR) <0.05 were considered statistically significant. In the DE analysis of the combined *Beclin1* cKO transcriptomic data, batch effects were adjusted for by including the batch in the edgeR design matrix.

Pathway enrichment analysis—Gene Set Enrichment Analysis (GSEA) with pre-ranked π values and default settings (with nperm=10000) were used to calculate the enriched Kyoto Encyclopedia of Genes and Genomes (KEGG) and Reactome pathways (MSigDB v6.2)[57]. Pathways with a nominal p-value <0.05 were considered statistically significant. π values were calculated based on a previous report[58].

Database search and data processing for proteomics—All mass spectra were processed using the Spectrum Mill software package v6.1 pre-release (Agilent Technologies), which includes modules developed by us for TMT10-based quantification. For peptide identification, MS/MS spectra were searched against the mouse Uniprot database to which a set of common laboratory contaminant proteins was supplemented. Search parameters included: ESI-QEXACTIVE-HCD scoring parameters, trypsin enzyme specificity with a maximum of two missed cleavages, 40% minimum matched peak intensity, +/− 20 ppm precursor mass tolerance, +/− 20 ppm product mass tolerance. Carbamidomethylation of cysteines and TMT10-Full labeling of lysines and peptide N-termini as fixed modifications. Allowed variable modifications were oxidation of methionine (M), acetyl (ProtN-term), and deamidated (N), with a precursor MH+ shift range of −18 to 64 Da. Identities interpreted for individual spectra were automatically designated as valid by optimizing score and delta rank1-rank2 score thresholds separately for each precursor charge state in each LC-MS/MS while allowing a maximum target-decoy-based false discovery rate (FDR) of 1.0% at the spectrum level.

TMT10 ratios were obtained from the protein-comparisons export table in Spectrum Mill. To obtain TMT10 protein ratios the median was calculated over all distinct peptides assigned to a protein subgroup in each replicate. To assign interacting proteins, we used the Limma package in the R environment and used multimedian analyses excluding the internal reference. Significantly different proteins were determined by moderated two-sample t-tests (Bland-Altman reproducibility analysis), and proteins in the top or bottom 5% logFC with an adjusted p-value <0.05 were considered significant.

Concordant and discordant features in transcriptomic and proteomic measurements—Concordant genes and proteins were defined as those with the same change direction observed at both the transcriptomic and proteomic levels, and with an absolute log fold change for both comparisons greater than $\log_2(1.2)$. Discordant genes and proteins were defined similarly, though with opposing change directions. Mixed genes and proteins exceeded these thresholds in transcriptomics or proteomics but not both.

Supplementary Material

Refer to Web version on PubMed Central for supplementary material.

Acknowledgments

We thank Herbert 'Skip' Virgin at Washington University in St. Louis for providing *Beclin1*$^{flox/flox}$-LysM-Cre^{+} and *Beclin1*$^{flox/flox}$-LysM-Cre^{-} mice, the late Beth Levine at University of Texas Southwestern for providing *Beclin1*$^{F121A/F121A}$ mice, and Brian K. Coombes at McMaster University for providing AIEC strain NRG857c. We thank Theresa Reimels for helping with the manuscript preparation, as well as Eric Chen and Karl Clauser for assistance with data deposition. This study was funded by the National Institutes of Health (R01DK097485, R01DK117263, U19AI109725, U19AI142784, and P30DK043351), The Leona M. and Harry B. Helmsley Charitable Trust, and the Klarman Cell Observatory at Broad Institute.

References

1. Medzhitov R (2008). Origin and physiological roles of inflammation. Nature 454, 428–435. 10.1038/nature07201. [PubMed: 18650913]
2. Netea MG, Balkwill F, Chonchol M, Cominelli F, Donath MY, Giamarellos-Bourboulis EJ, Golenbock D, Gresnigt MS, Heneka MT, Hoffman HM, et al. (2017). A guiding map for inflammation. Nat Immunol 18, 826–831. 10.1038/ni.3790. [PubMed: 28722720]
3. Meizlish ML, Franklin RA, Zhou X, and Medzhitov R (2021). Tissue Homeostasis and Inflammation. Annu Rev Immunol 39, 557–581. 10.1146/annurev-immunol-061020-053734. [PubMed: 33651964]
4. Matsuzawa-Ishimoto Y, Hwang S, and Cadwell K (2018). Autophagy and Inflammation. Annu Rev Immunol 36, 73–101. 10.1146/annurev-immunol-042617-053253. [PubMed: 29144836]
5. Levine B, Mizushima N, and Virgin HW (2011). Autophagy in immunity and inflammation. Nature 469, 323–335. 10.1038/nature09782. [PubMed: 21248839]
6. Shibutani ST, Saitoh T, Nowag H, Munz C, and Yoshimori T (2015). Autophagy and autophagy-related proteins in the immune system. Nat Immunol 16, 1014–1024. 10.1038/ni.3273. [PubMed: 26382870]
7. Lu Q, Yokoyama CC, Williams JW, Baldridge MT, Jin X, DesRochers B, Bricker T, Wilen CB, Bagaitkar J, Loginicheva E, et al. (2016). Homeostatic Control of Innate Lung Inflammation by Vici Syndrome Gene Epg5 and Additional Autophagy Genes Promotes Influenza Pathogenesis. Cell Host Microbe 19, 102–113. 10.1016/j.chom.2015.12.011. [PubMed: 26764600]
8. Park S, Buck MD, Desai C, Zhang X, Loginicheva E, Martinez J, Freeman ML, Saitoh T, Akira S, Guan JL, et al. (2016). Autophagy Genes Enhance Murine Gammaherpesvirus 68 Reactivation from Latency by Preventing Virus-Induced Systemic Inflammation. Cell Host Microbe 19, 91–101. 10.1016/j.chom.2015.12.010. [PubMed: 26764599]
9. Marino G, Niso-Santano M, Baehrecke EH, and Kroemer G (2014). Self-consumption: the interplay of autophagy and apoptosis. Nat Rev Mol Cell Biol 15, 81–94. 10.1038/nrm3735. [PubMed: 24401948]
10. Ravichandran KS (2010). Find-me and eat-me signals in apoptotic cell clearance: progress and conundrums. J Exp Med 207, 1807–1817. 10.1084/jem.20101157. [PubMed: 20805564]
11. Nakahira K, Haspel JA, Rathinam VA, Lee SJ, Dolinay T, Lam HC, Englert JA, Rabinovitch M, Cernadas M, Kim HP, et al. (2011). Autophagy proteins regulate innate immune responses by inhibiting the release of mitochondrial DNA mediated by the NALP3 inflammasome. Nat Immunol 12, 222–230. 10.1038/ni.1980. [PubMed: 21151103]
12. Liu T, Tang Q, Liu K, Xie W, Liu X, Wang H, Wang RF, and Cui J (2016). TRIM11 Suppresses AIM2 Inflammasome by Degrading AIM2 via p62-Dependent Selective Autophagy. Cell Rep 16, 1988–2002. 10.1016/j.celrep.2016.07.019. [PubMed: 27498865]
13. Saitoh T, Fujita N, Jang MH, Uematsu S, Yang BG, Satoh T, Omori H, Noda T, Yamamoto N, Komatsu M, et al. (2008). Loss of the autophagy protein Atg16L1 enhances endotoxin-induced IL-1beta production. Nature 456, 264–268. 10.1038/nature07383. [PubMed: 18849965]
14. Netea-Maier RT, Plantinga TS, van de Veerdonk FL, Smit JW, and Netea MG (2016). Modulation of inflammation by autophagy: Consequences for human disease. Autophagy 12, 245–260. 10.1080/15548627.2015.1071759. [PubMed: 26222012]
15. Shi CS, Shenderov K, Huang NN, Kabat J, Abu-Asab M, Fitzgerald KA, Sher A, and Kehrl JH (2012). Activation of autophagy by inflammatory signals limits IL-1beta production by

targeting ubiquitinated inflammasomes for destruction. Nat Immunol 13, 255–263. 10.1038/ni.2215. [PubMed: 22286270]

16. Liang XH, Kleeman LK, Jiang HH, Gordon G, Goldman JE, Berry G, Herman B, and Levine B (1998). Protection against fatal Sindbis virus encephalitis by beclin, a novel Bcl-2-interacting protein. J Virol 72, 8586–8596. 10.1128/JVI.72.11.8586-8596.1998. [PubMed: 9765397]
17. Liang XH, Jackson S, Seaman M, Brown K, Kempkes B, Hibshoosh H, and Levine B (1999). Induction of autophagy and inhibition of tumorigenesis by beclin 1. Nature 402, 672–676. 10.1038/45257. [PubMed: 10604474]
18. Funderburk SF, Wang QJ, and Yue Z (2010). The Beclin 1-VPS34 complex--at the crossroads of autophagy and beyond. Trends Cell Biol 20, 355–362. 10.1016/j.tcb.2010.03.002. [PubMed: 20356743]
19. Yue Z, Jin S, Yang C, Levine AJ, and Heintz N (2003). Beclin 1, an autophagy gene essential for early embryonic development, is a haploinsufficient tumor suppressor. Proc Natl Acad Sci U S A 100, 15077–15082. 10.1073/pnas.2436255100. [PubMed: 14657337]
20. Qu X, Yu J, Bhagat G, Furuya N, Hibshoosh H, Troxel A, Rosen J, Eskelinen EL, Mizushima N, Ohsumi Y, et al. (2003). Promotion of tumorigenesis by heterozygous disruption of the beclin 1 autophagy gene. J Clin Invest 112, 1809–1820. 10.1172/JCI20039. [PubMed: 14638851]
21. Levine B, and Klionsky DJ (2017). Autophagy wins the 2016 Nobel Prize in Physiology or Medicine: Breakthroughs in baker's yeast fuel advances in biomedical research. Proc Natl Acad Sci U S A 114, 201–205. 10.1073/pnas.1619876114. [PubMed: 28039434]
22. Gawriluk TR, Hale AN, Flaws JA, Dillon CP, Green DR, and Rucker EB 3rd (2011). Autophagy is a cell survival program for female germ cells in the murine ovary. Reproduction 141, 759–765. 10.1530/REP-10-0489. [PubMed: 21464117]
23. Wang YT, Sansone A, Smirnov A, Stallings CL, and Orvedahl A (2022). Myeloid autophagy genes protect mice against fatal TNF- and LPS-induced cytokine storm syndromes. Autophagy, 1–14. 10.1080/15548627.2022.2116675.
24. Leonard A, Millar MW, Slavin SA, Bijli KM, Dionisio Santos DA, Dean DA, Fazal F, and Rahman A (2019). Critical role of autophagy regulator Beclin1 in endothelial cell inflammation and barrier disruption. Cell Signal 61, 120–129. 10.1016/j.cellsig.2019.04.013. [PubMed: 31054328]
25. Rocchi A, Yamamoto S, Ting T, Fan Y, Sadleir K, Wang Y, Zhang W, Huang S, Levine B, Vassar R, and He C (2017). A Becn1 mutation mediates hyperactive autophagic sequestration of amyloid oligomers and improved cognition in Alzheimer's disease. PLoS Genet 13, e1006962. 10.1371/journal.pgen.1006962. [PubMed: 28806762]
26. Fernandez AF, Sebti S, Wei Y, Zou Z, Shi M, McMillan KL, He C, Ting T, Liu Y, Chiang WC, et al. (2018). Disruption of the beclin 1-BCL2 autophagy regulatory complex promotes longevity in mice. Nature 558, 136–140. 10.1038/s41586-018-0162-7. [PubMed: 29849149]
27. Kuramoto K, Kim YJ, Hong JH, and He C (2021). The autophagy protein Becn1 improves insulin sensitivity by promoting adiponectin secretion via exocyst binding. Cell Rep 35, 109184. 10.1016/j.celrep.2021.109184. [PubMed: 34038729]
28. Behrens EM, Canna SW, Slade K, Rao S, Kreiger PA, Paessler M, Kambayashi T, and Koretzky GA (2011). Repeated TLR9 stimulation results in macrophage activation syndrome-like disease in mice. J Clin Invest 121, 2264–2277. 10.1172/JCI43157. [PubMed: 21576823]
29. Weaver LK, Minichino D, Biswas C, Chu N, Lee JJ, Bittinger K, Albeituni S, Nichols KE, and Behrens EM (2019). Microbiota-dependent signals are required to sustain TLR-mediated immune responses. JCI Insight 4. 10.1172/jci.insight.124370.
30. Koulnis M, Pop R, Porpiglia E, Shearstone JR, Hidalgo D, and Socolovsky M (2011). Identification and analysis of mouse erythroid progenitors using the CD71/TER119 flow-cytometric assay. J Vis Exp. 10.3791/2809.
31. Tang Y, Xu X, Song H, Yang S, Shi S, Wei J, Pan B, Zhao F, Liao C, and Luo C (2008). Early diagnostic and prognostic significance of a specific Th1/Th2 cytokine pattern in children with haemophagocytic syndrome. Br J Haematol 143, 84–91. 10.1111/j.1365-2141.2008.07298.x. [PubMed: 18673367]

32. Jordan MB, Hildeman D, Kappler J, and Marrack P (2004). An animal model of hemophagocytic lymphohistiocytosis (HLH): CD8+ T cells and interferon gamma are essential for the disorder. Blood 104, 735–743. 10.1182/blood-2003-10-3413. [PubMed: 15069016]
33. Tracey KJ, Beutler B, Lowry SF, Merryweather J, Wolpe S, Milsark IW, Hariri RJ, Fahey TJ 3rd, Zentella A, Albert JD, and et al. (1986). Shock and tissue injury induced by recombinant human cachectin. Science 234, 470–474. 10.1126/science.3764421. [PubMed: 3764421]
34. Schulert GS, and Grom AA (2014). Macrophage activation syndrome and cytokine-directed therapies. Best Pract Res Clin Rheumatol 28, 277–292. 10.1016/j.berh.2014.03.002. [PubMed: 24974063]
35. Deretic V, and Levine B (2009). Autophagy, immunity, and microbial adaptations. Cell Host Microbe 5, 527–549. 10.1016/j.chom.2009.05.016. [PubMed: 19527881]
36. Palmela C, Chevarin C, Xu Z, Torres J, Sevrin G, Hirten R, Barnich N, Ng SC, and Colombel JF (2018). Adherent-invasive Escherichia coli in inflammatory bowel disease. Gut 67, 574–587. 10.1136/gutjnl-2017-314903. [PubMed: 29141957]
37. Darfeuille-Michaud A, Boudeau J, Bulois P, Neut C, Glasser AL, Barnich N, Bringer MA, Swidsinski A, Beaugerie L, and Colombel JF (2004). High prevalence of adherent-invasive Escherichia coli associated with ileal mucosa in Crohn's disease. Gastroenterology 127, 412–421. 10.1053/j.gastro.2004.04.061. [PubMed: 15300573]
38. Lapaquette P, Glasser AL, Huett A, Xavier RJ, and Darfeuille-Michaud A (2010). Crohn's disease-associated adherent-invasive E. coli are selectively favoured by impaired autophagy to replicate intracellularly. Cell Microbiol 12, 99–113. 10.1111/j.1462-5822.2009.01381.x. [PubMed: 19747213]
39. Elhenawy W, Tsai CN, and Coombes BK (2019). Host-Specific Adaptive Diversification of Crohn's Disease-Associated Adherent-Invasive Escherichia coli. Cell Host Microbe 25, 301–312 e305. 10.1016/j.chom.2018.12.010. [PubMed: 30683582]
40. Hu X, Deng J, Yu T, Chen S, Ge Y, Zhou Z, Guo Y, Ying H, Zhai Q, Chen Y, et al. (2019). ATF4 Deficiency Promotes Intestinal Inflammation in Mice by Reducing Uptake of Glutamine and Expression of Antimicrobial Peptides. Gastroenterology 156, 1098–1111. 10.1053/j.gastro.2018.11.033. [PubMed: 30452920]
41. Jeong SY, Im YN, Youm JY, Lee HK, and Im SY (2018). l-Glutamine Attenuates DSS-Induced Colitis via Induction of MAPK Phosphatase-1. Nutrients 10. 10.3390/nu10030288.
42. Liu PS, Wang H, Li X, Chao T, Teav T, Christen S, Di Conza G, Cheng WC, Chou CH, Vavakova M, et al. (2017). alpha-ketoglutarate orchestrates macrophage activation through metabolic and epigenetic reprogramming. Nat Immunol 18, 985–994. 10.1038/ni.3796. [PubMed: 28714978]
43. Song G, Liu B, Li Z, Wu H, Wang P, Zhao K, Jiang G, Zhang L, and Gao C (2016). E3 ubiquitin ligase RNF128 promotes innate antiviral immunity through K63-linked ubiquitination of TBK1. Nat Immunol 17, 1342–1351. 10.1038/ni.3588. [PubMed: 27776110]
44. Soulat D, Burckstummer T, Westermayer S, Goncalves A, Bauch A, Stefanovic A, Hantschel O, Bennett KL, Decker T, and Superti-Furga G (2008). The DEAD-box helicase DDX3X is a critical component of the TANK-binding kinase 1-dependent innate immune response. EMBO J 27, 2135–2146. 10.1038/emboj.2008.126. [PubMed: 18583960]
45. Wild P, Farhan H, McEwan DG, Wagner S, Rogov VV, Brady NR, Richter B, Korac J, Waidmann O, Choudhary C, et al. (2011). Phosphorylation of the autophagy receptor optineurin restricts Salmonella growth. Science 333, 228–233. 10.1126/science.1205405. [PubMed: 21617041]
46. Yang S, Imamura Y, Jenkins RW, Canadas I, Kitajima S, Aref A, Brannon A, Oki E, Castoreno A, Zhu Z, et al. (2016). Autophagy Inhibition Dysregulates TBK1 Signaling and Promotes Pancreatic Inflammation. Cancer Immunol Res 4, 520–530. 10.1158/2326-6066.CIR-15-0235. [PubMed: 27068336]
47. Goodwin JM, Dowdle WE, DeJesus R, Wang Z, Bergman P, Kobylarz M, Lindeman A, Xavier RJ, McAllister G, Nyfeler B, et al. (2017). Autophagy-Independent Lysosomal Targeting Regulated by ULK1/2-FIP200 and ATG9. Cell Rep 20, 2341–2356. 10.1016/j.celrep.2017.08.034. [PubMed: 28877469]

48. Franceschi C, Garagnani P, Parini P, Giuliani C, and Santoro A (2018). Inflammaging: a new immune-metabolic viewpoint for age-related diseases. Nat Rev Endocrinol 14, 576–590. 10.1038/s41574-018-0059-4. [PubMed: 30046148]

49. Maculins T, Verschueren E, Hinkle T, Choi M, Chang P, Chalouni C, Rao S, Kwon Y, Lim J, Katakam AK, et al. (2021). Multiplexed proteomics of autophagy-deficient murine macrophages reveals enhanced antimicrobial immunity via the oxidative stress response. Elife 10. 10.7554/eLife.62320.

50. O'Neill LA, and Pearce EJ (2016). Immunometabolism governs dendritic cell and macrophage function. J Exp Med 213, 15–23. 10.1084/jem.20151570. [PubMed: 26694970]

51. Kumar S, Gu Y, Abudu YP, Bruun JA, Jain A, Farzam F, Mudd M, Anonsen JH, Rusten TE, Kasof G, et al. (2019). Phosphorylation of Syntaxin 17 by TBK1 Controls Autophagy Initiation. Dev Cell 49, 130–144 e136. 10.1016/j.devcel.2019.01.027. [PubMed: 30827897]

52. Pilli M, Arko-Mensah J, Ponpuak M, Roberts E, Master S, Mandell MA, Dupont N, Ornatowski W, Jiang S, Bradfute SB, et al. (2012). TBK-1 promotes autophagy-mediated antimicrobial defense by controlling autophagosome maturation. Immunity 37, 223–234. 10.1016/j.immuni.2012.04.015. [PubMed: 22921120]

53. Liu Y, Nguyen PT, Wang X, Zhao Y, Meacham CE, Zou Z, Bordieanu B, Johanns M, Vertommen D, Wijshake T, et al. (2020). TLR9 and beclin 1 crosstalk regulates muscle AMPK activation in exercise. Nature 578, 605–609. 10.1038/s41586-020-1992-7. [PubMed: 32051584]

54. Kim D, Pertea G, Trapnell C, Pimentel H, Kelley R, and Salzberg SL (2013). TopHat2: accurate alignment of transcriptomes in the presence of insertions, deletions and gene fusions. Genome Biol 14, R36. 10.1186/gb-2013-14-4-r36. [PubMed: 23618408]

55. Anders S, Pyl PT, and Huber W (2015). HTSeq--a Python framework to work with high-throughput sequencing data. Bioinformatics 31, 166–169. 10.1093/bioinformatics/btu638. [PubMed: 25260700]

56. Robinson MD, McCarthy DJ, and Smyth GK (2010). edgeR: a Bioconductor package for differential expression analysis of digital gene expression data. Bioinformatics 26, 139–140. 10.1093/bioinformatics/btp616. [PubMed: 19910308]

57. Subramanian A, Tamayo P, Mootha VK, Mukherjee S, Ebert BL, Gillette MA, Paulovich A, Pomeroy SL, Golub TR, Lander ES, and Mesirov JP (2005). Gene set enrichment analysis: a knowledge-based approach for interpreting genome-wide expression profiles. Proc Natl Acad Sci U S A 102, 15545–15550. 10.1073/pnas.0506580102. [PubMed: 16199517]

58. Xiao Y, Hsiao TH, Suresh U, Chen HI, Wu X, Wolf SE, and Chen Y (2014). A novel significance score for gene selection and ranking. Bioinformatics 30, 801–807. 10.1093/bioinformatics/btr671. [PubMed: 22321699]

Highlights

- Autophagy can dampen cytokine production during hyperinflammation and infection
- Proteogenomics reveal reduced *Slc7a11* mRNA and RNF128 protein with increased flux
- *Slc7a11* knockdown suppresses cytokine increase in Beclin1-deficient macrophages
- *Rnf128* loss reduces type I interferon and IL-12ß in Beclin1-deficient macrophages

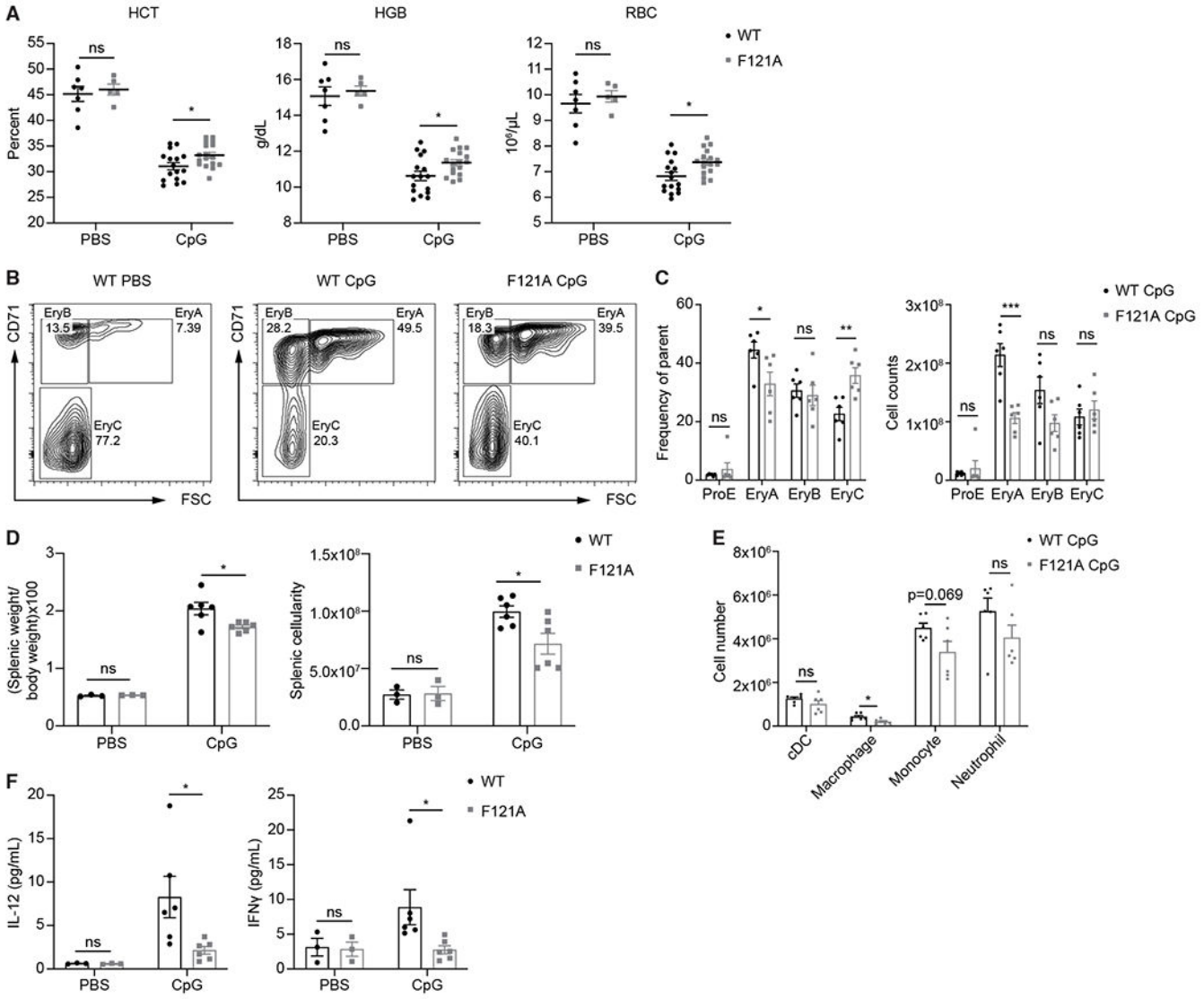

Figure 1. The Beclin1 F121A variant ameliorates anemia and inflammation in a model of macrophage activation syndrome.

Mice were treated with intraperitoneal injections of PBS or CpG (50 μg) on days 0, 2, 4, 7 and 9. **(A)** Blood was collected on day 8 for a complete blood count and analyzed for anemia (HCT, hematocrit; HGB, total hemoglobin; RBC, red blood cell). **(B)** Erythrocyte progenitor state in the mouse spleen was evaluated by considering CD71 expression and FSC levels among Ter119^{+} cells. Contour plots displayed were first gated on single cells, viable cells, and Ter119^{+} cells. The erythroblastic precursor ProE is defined as Ter119^{med}CD71^{high}. **(C)** Frequency and absolute number of erythroid progenitors from B. **(D)** Splenic weight in the indicated conditions was normalized to body weight (left) and total splenocyte numbers were measured (right). **(E)** Cell counts of conventional DCs (cDCs), macrophages, monocytes, and neutrophils in the spleen. **(F)** Serum cytokines were measured on day 10 after CpG treatment. Data in A are mean with SEM pooled from 3 individual experiments. n=7 (WT, PBS), n=5 (F121A, PBS), n=16 (WT, CpG), and n=17 (F121A, CpG) mice. Data in C-F are mean with SEM representative of 3 individual experiments. n=3 (WT, PBS), n=3

(F121A, PBS), n=6 (WT, CpG), and n=6 (F121A, CpG) mice. Individual symbols represent 1 mouse. Unpaired t-tests were used in A, C and E. One-way ANOVA was used in D and F. ns=not significant, *p<0.05, **p<0.01, ***p<0.001. See also Figure S1 and S2.

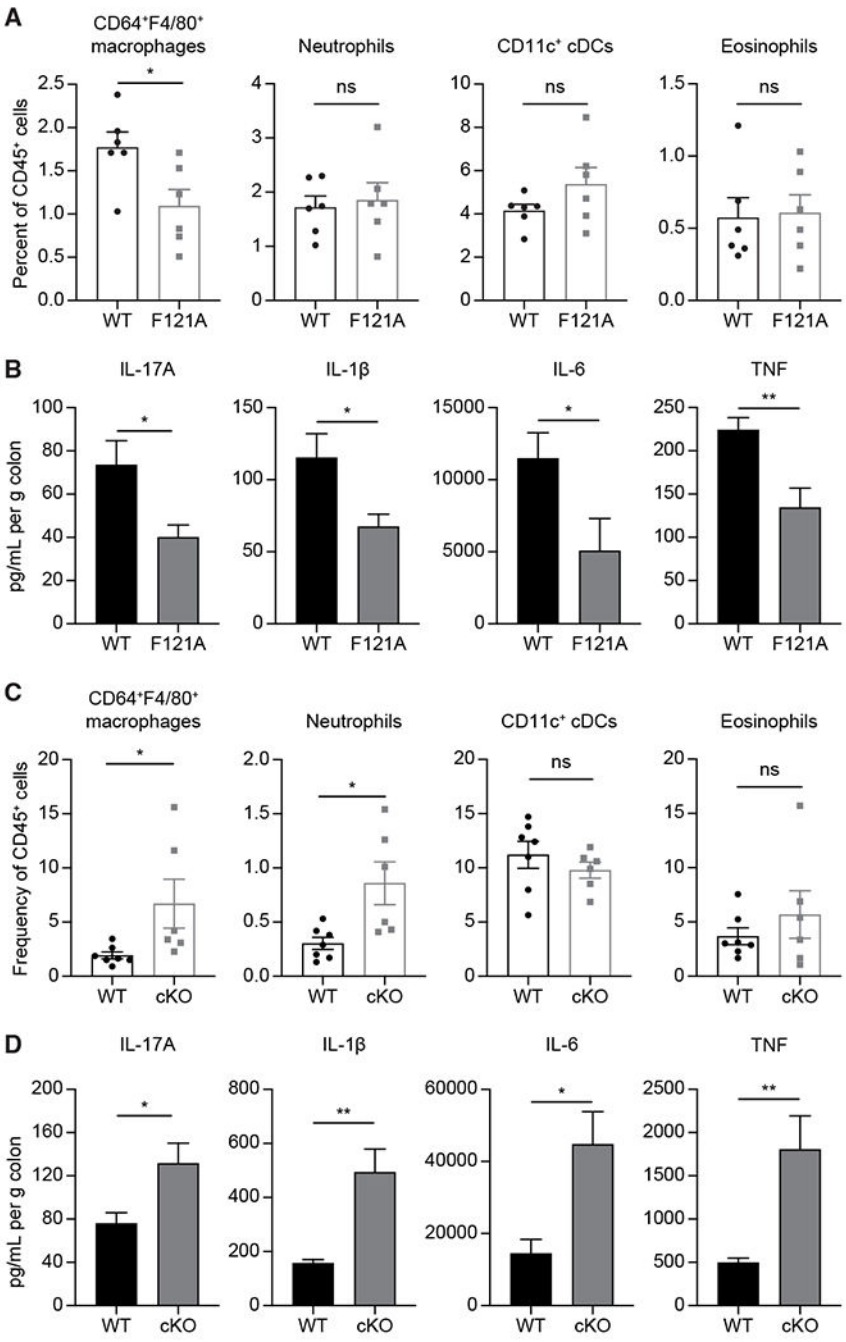

Figure 2. Beclin1 activity modulates intestinal inflammation in mice infected with AIEC.

(A) Frequency of macrophages, neutrophils, cDCs and eosinophils in the colons of *Beclin1* F121A mice and WT littermates 2 days after infection. **(B)** Cytokine levels in the media of WT and F121A explanted colons cultured for 24 hours. Colons were isolated from mice 2 days after AIEC infection. **(C)** Frequency of macrophages, neutrophils, cDCs and eosinophils in the colons of *Beclin1* cKO mice and WT littermates 2 days after infection. **(D)** Cytokine levels in the media of WT and cKO colons cultured for 24 hours, isolated from mice 2 days post infection. Data in A and B are mean with SEM representative of

2 individual experiments, n=5-6 mice per genotype. Data in C and D are mean with SEM combined from 2 individual experiments, n=6-8 mice per genotype. ns=not significant, *p<0.05, **p<0.01; unpaired t-test. See also Figure S3.

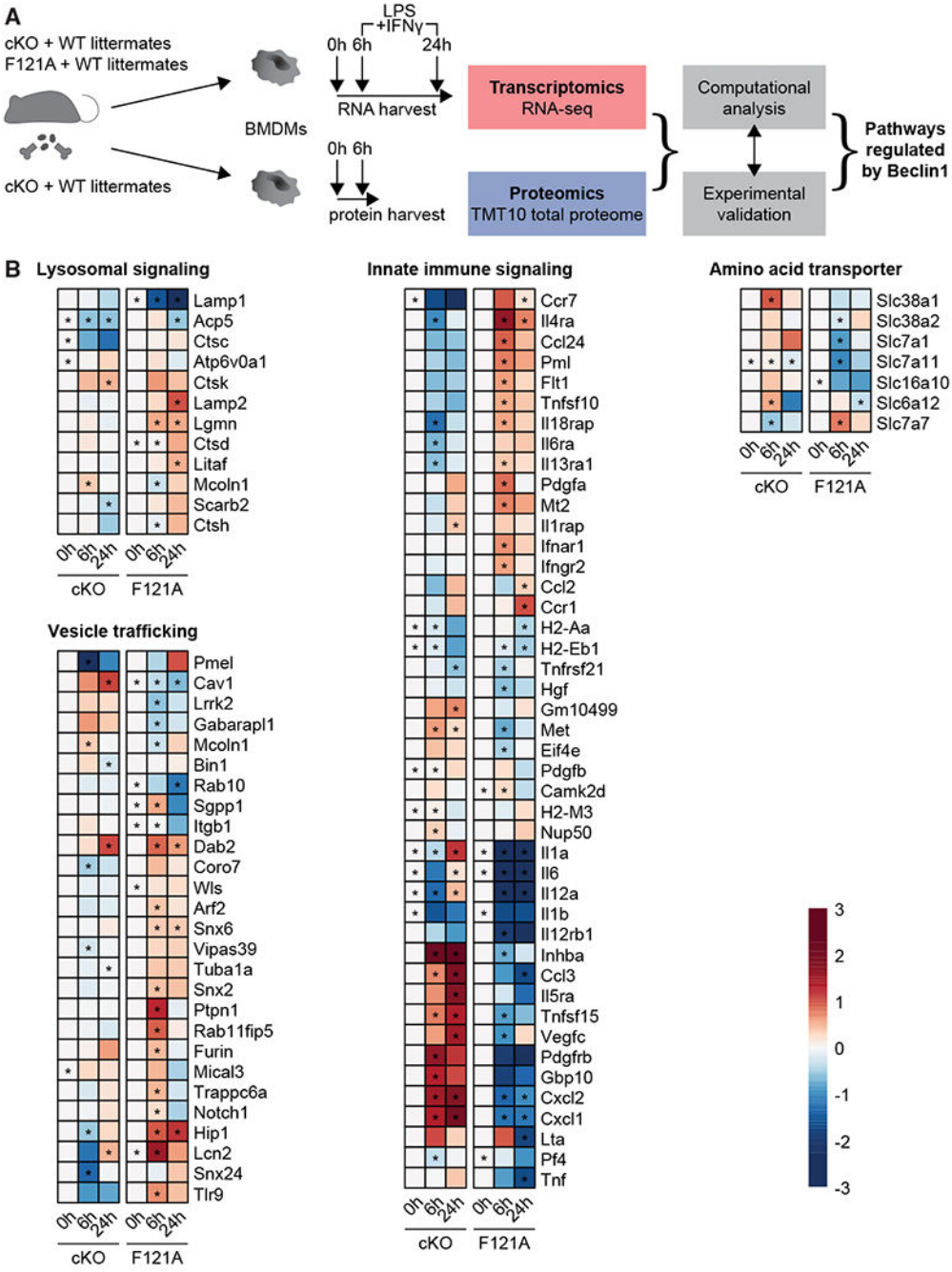

Figure 3. Proteogenomics workflow and overview of differentially expressed genes.

(A) Workflow. Bone marrow was collected from cKO mice, F121A mice, and corresponding WT littermate controls and cultured in media with M-CSF for 7 days to generate BMDMs. WT and cKO BMDMs as well as WT and F121A BMDMs were unstimulated (0h) or treated with LPS plus IFNγ for the indicated times prior to transcriptomic or proteogenomic analysis. **(B)** Heatmap ($\log_2$ fold change) of genes involved in selected pathways showing strong concordance between cKO and F121A transcriptomes. *FDR<0.05. Before comparing WT and cKO transcriptomics, WT 6h or 24h values were normalized to WT

0h values and cKO 6h or 24h values were normalized to KO 0h values. The same normalizations were performed for WT and F121A transcriptomics before comparing. See also Figure S4, Table S1.

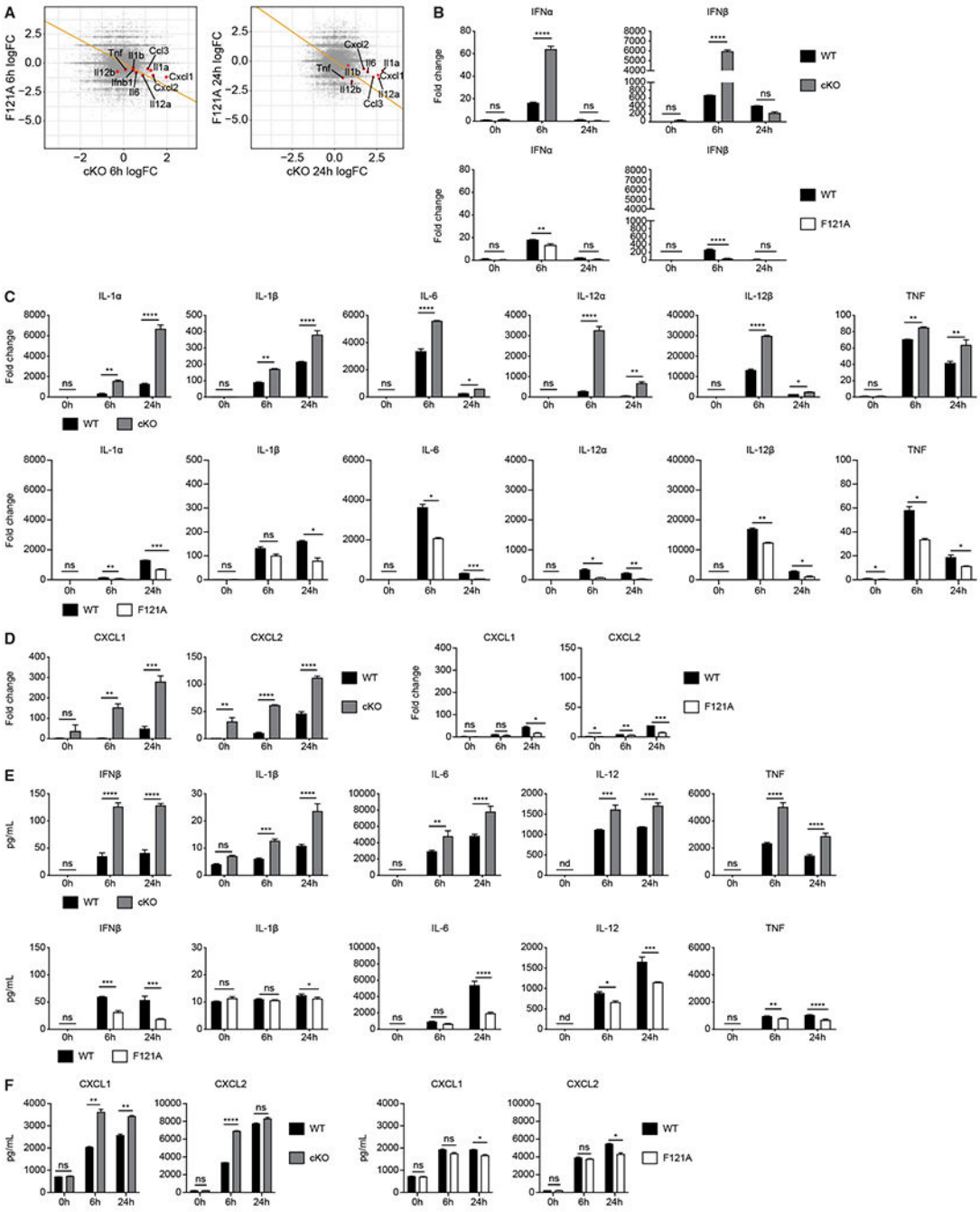

Figure 4. Beclin1 regulates inflammatory cytokines, type I interferon, and chemokines.

(A) Scatterplots of the log fold change (FC) in cKO BMDMs (normalized to WT) versus the logFC in F121A BMDMs (normalized to WT) of all genes at 6h and 24h after LPS+IFNγ treatment. Cytokine genes are represented in red, the expected trend of an opposite FC between F121A and cKO BMDMs is represented in orange. **(B-D)** Expression of type I interferon (B), cytokines (C), and chemokines (D) in LPS+IFNγ-treated WT and cKO or WT and F121A BMDMs, as measured by qRT-PCR. mRNA levels relative to unstimulated WT cells are shown. **(E, F)** Secretion of type I interferon, cytokines (E) and chemokines

(F) was measured in LPS+IFNγ-treated WT and cKO or WT and F121A BMDMs. Data in B–F are mean with SEM representative of 3 independent experiments (n=2-4 per genotype per experiment). nd=not detected, ns=not significant, *p<0.05, **p<0.01, ***p<0.001, ****p<0.0001; multiple unpaired t-test.

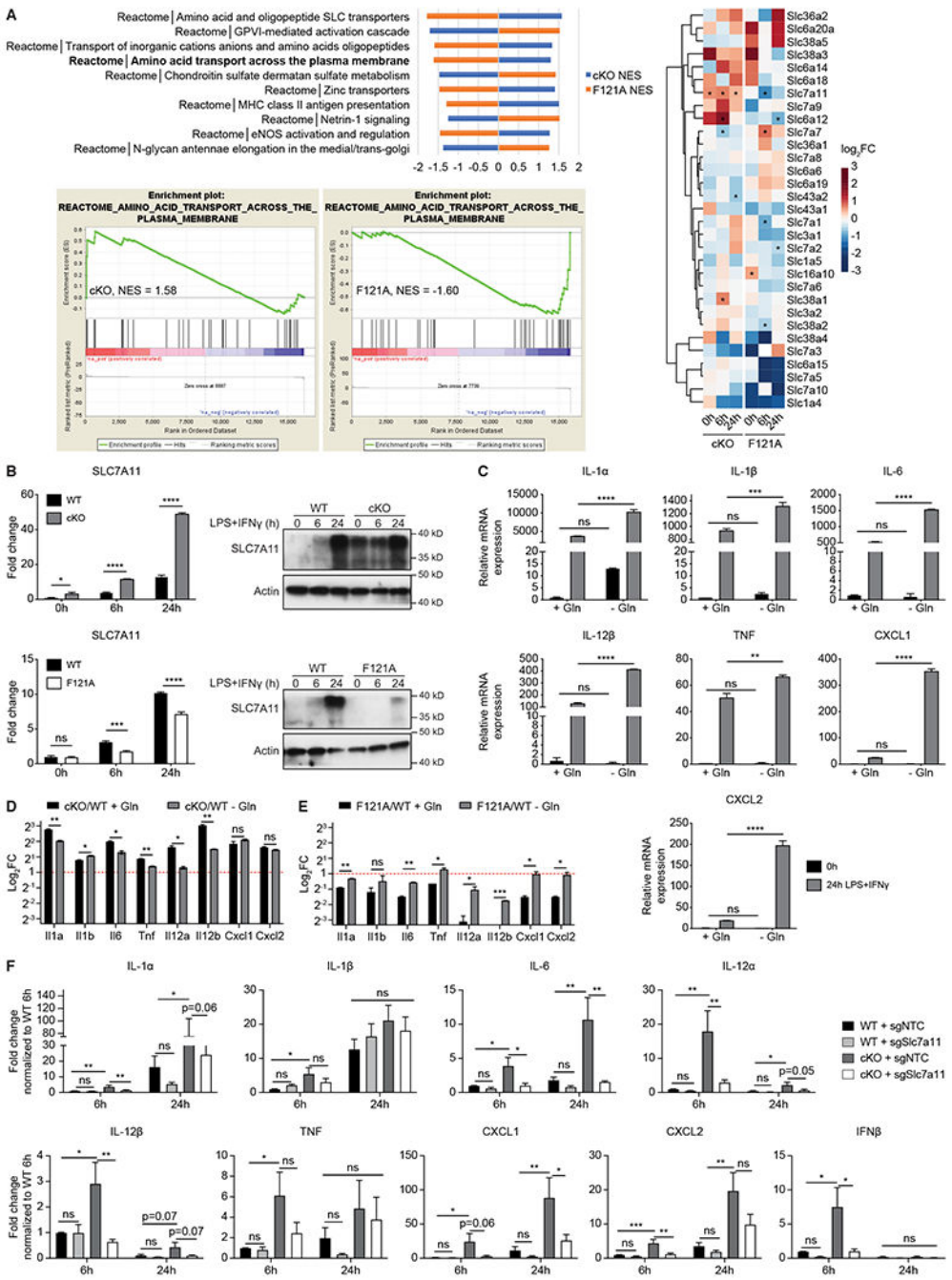

Figure 5. Beclin1 regulates inflammation through glutamine/glutathione metabolism.

(A) Normalized enrichment scores (NES) for the top 10 Reactome pathways with opposite enrichment scores in *Beclin1* cKO and F121A BMDMs (top left, Methods) and representative GSEA enrichment plots for Reactome "Amino acid transport across the plasma membrane" pathway in both cKO and F121A BMDMs (bottom left). The heatmap shows the $\log_2$FC of genes involved in this pathway (right). *FDR<0.05. **(B)** qRT-PCR (left) and western blot (right) analysis in cKO, F121A, and corresponding WT BMDMs stimulated with LPS+IFNγ. **(C)** qRT-PCR analysis of mRNA expression of

proinflammatory mediators in WT BMDMs stimulated with LPS+IFNγ for 24h with and without glutamine. Glutamine deprivation markedly increased cytokines levels in stimulated cells. **(D, E)** Glutamine deprivation rescues differences in the levels of cytokines and chemokines between WT and *Beclin1* cKO BMDMs (D) and between WT and *Beclin1* F121A BMDMs (E). Red dotted lines represent no difference between WT and cKO or WT and F121A BMDMs. **(F)** qRT-PCR analysis of proinflammatory mediators with CRISPR-Cas9-mediated reduction of *Slc7a11* in WT and cKO BMDMs. Data in B-E are mean with SEM representative of at least 2 independent experiments (n=2 per genotype per experiment). Data in F are mean with SEM pooled from 3-5 individual experiments (n=6-10 per group). ns=not significant, *p<0.05, **p<0.01, ***p<0.001, ****p<0.0001; Multiple unpaired t-test in B; one-way ANOVA in C and F; unpaired t-test in D and E. See also Figure S5.

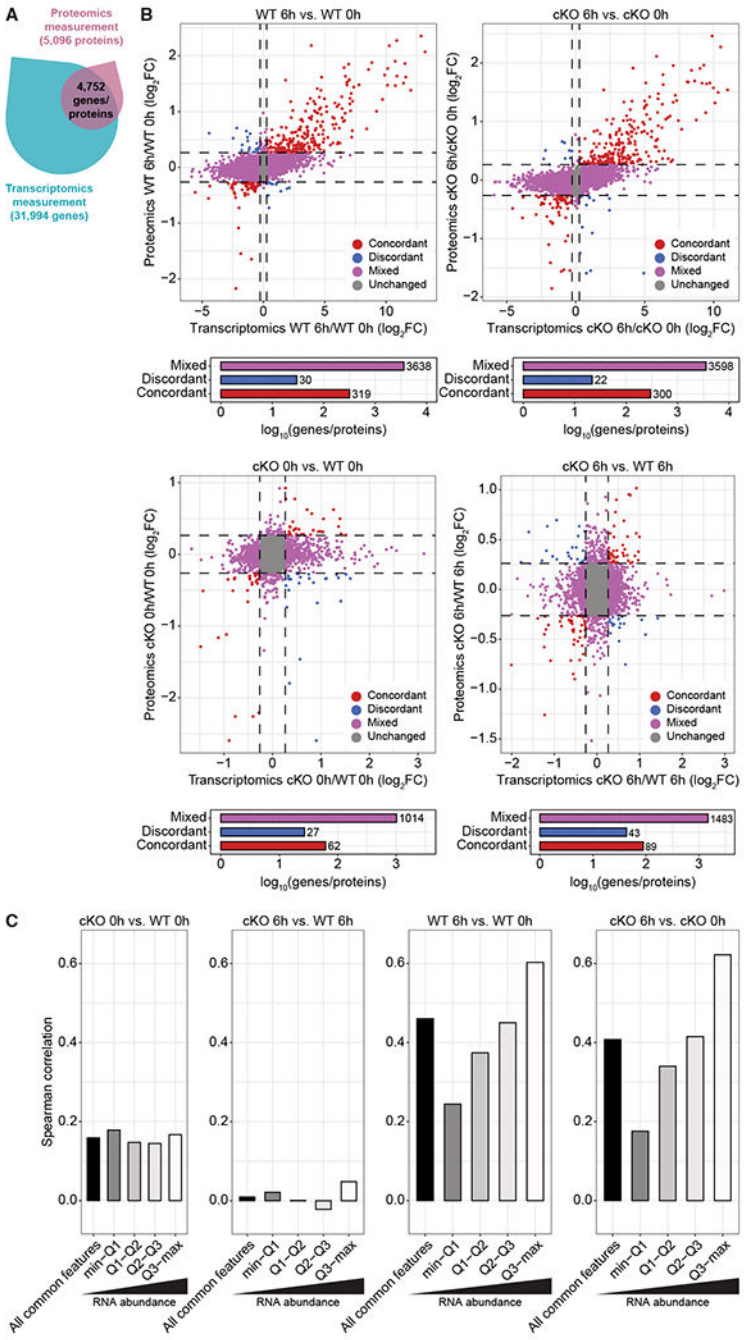

Figure 6. The effects of Beclin1 deficiency on gene expression have low concordance in proteomics.

(A) Venn diagram of total unique genes/proteins measured from transcriptomics and proteomics of WT and *Beclin1* cKO BMDMs. **(B)** Scatter plots show $\log_2$FC of 4,752 common features detected in proteomics versus transcriptomics. Dashed lines denote FC=±1.2. Barplots show the number of each type of feature in the scatter plot above. **(C)** Spearman's correlation of logFC in RNA versus protein. Genes were divided into 4 quartiles (min-Q1, Q1-Q2, Q2-Q3, and Q3-max) based on the mean log counts per million (CPM)

measure by transcriptomics, and the correlation between transcriptomic and proteomic FCs was evaluated for this subset. See also Figure S6.

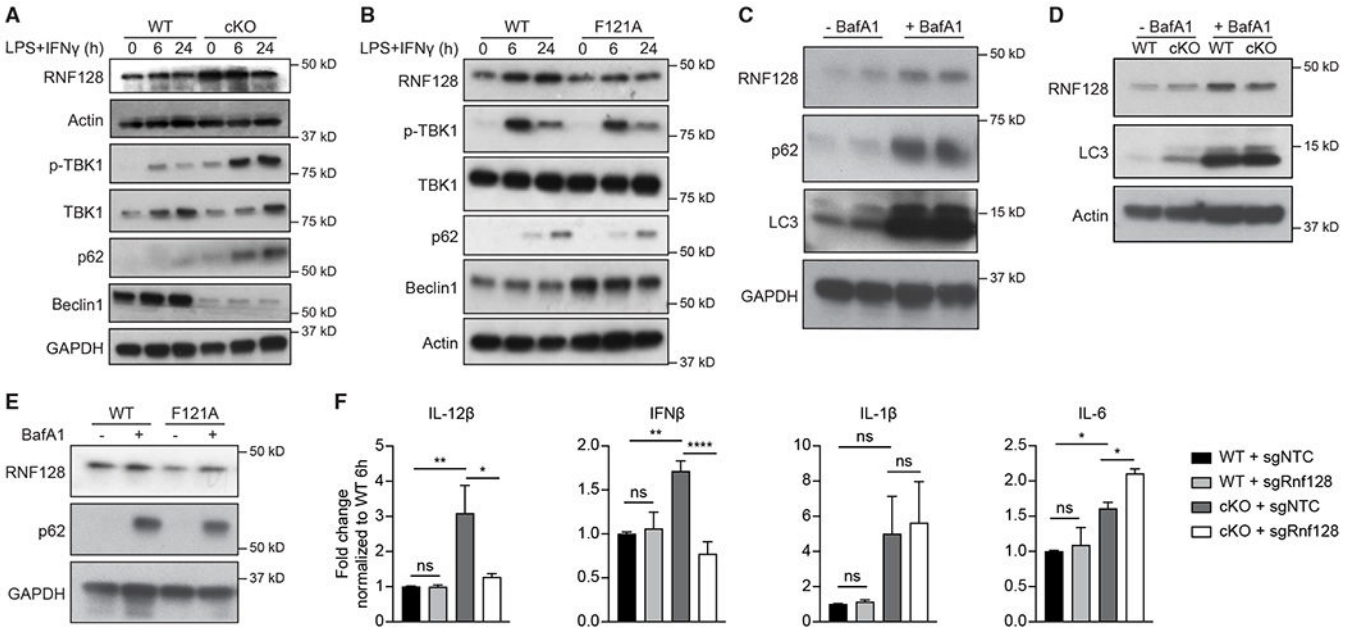

Figure 7. Beclin1 regulates inflammatory mediators in an RNF128/TBK1-dependent manner.

(A, B) Beclin1 regulates protein levels of RNF128 and activation of TBK1. Immunoblots of lysates from WT and *Beclin1* cKO BMDMs (A) and WT and *Beclin1* F121A BMDMs (B) treated with LPS+IFNγ for the indicated times. TBK1 phosphorylation (p-TBK1) was detected by an anti-phospho-TBK1 (Ser172) antibody. **(C)** RNF128 levels in WT BMDMs increased after bafilomycin A1 (BafA1, 100nM) treatment for 4 hours. **(D, E)** BafA1 attenuates the differences in RNF128 levels between WT and *Beclin1* cKO BMDMs (D) and between WT and *Beclin1* F121A BMDMs (E). **(F)** qRT-PCR analysis of proinflammatory mediators with CRISPR-Cas9-mediated reduction of *Rnf128* in WT and cKO BMDMs after treatment with LPS+IFNγ for 6h. Data in A-E are representative of at least 2 independent experiments. Data in F are mean with SEM pooled from 3 individual experiments (n=8 per group). ns=not significant, ** p<0.01, *** p<0.001, **** p<0.0001; one-way ANOVA. See also Figure S7, Table S2.

Key resources table

REAGENT or RESOURCE	SOURCE	IDENTIFIER
Antibodies		
Biotin-CD3	BioLegend	Cat# 100303, RRID:AB_312668
Biotin-B220	BioLegend	Cat# 103204, RRID:AB_312989
Biotin-CD11b	BioLegend	Cat# 101204, RRID:AB_312787
Biotin-Gr-1	BioLegend	Cat# 108404, RRID:AB_313369
Biotin-F4/80	BioLegend	Cat# 123106, RRID:AB_893501
Biotin-CD11c	BioLegend	Cat# 117304, RRID:AB_313773
Biotin-NK1.1	BioLegend	Cat# 108703, RRID:AB_313390
CD71	BioLegend	Cat# 113812, RRID:AB_2203382
Ter119	BioLegend	Cat# 116234, RRID:AB_2562917
APC Streptavidin	BioLegend	Cat# 405207
Live/dead fixable Zombie UV dye	BioLegend	Cat# 423108
CD19	BioLegend	Cat# 115521, RRID:AB_389307
CD11b	BioLegend	Cat# 101243, RRID:AB_2561373
F4/80	BioLegend	Cat# 123117, RRID:AB_893489
Ly6G	BioLegend	Cat# 127610, RRID:AB_312989
CD11c	BioLegend	Cat# 117339, RRID:AB_2562414
CD3e	BD Biosciences	Cat# 563565, RRID:AB_2738278
CD8a	BioLegend	Cat# 100752, RRID:AB_2563057
CD4	BD Biosciences	Cat# 553653, RRID:AB_394973
CD45	BD Biosciences	Cat# 103128, RRID:AB_493715
MHCII	BioLegend	Cat# 107639, RRID:AB_2565894
MHCII	BioLegend	Cat# 107620, RRID:AB_493527
F4/80	BioLegend	Cat# 123120, RRID:AB_893479
CD64	BioLegend	Cat# 139306, RRID:AB_11219391
CD11c	BioLegend	Cat# 117318, RRID:AB_493568
CD11b	BioLegend	Cat# 101262, RRID:AB_2572122
SiglecF	BD Biosciences	Cat# 562757, RRID:AB_2687994
Ly6G	BioLegend	Cat# 127633, RRID:AB_2562937
Beclin-1	Cell Signaling Technology	Cat#3495 RRID:AB_1903911
RNF128	Abcam	Cat# ab137088
TBK1	Cell Signaling Technology	Cat# 3504, RRID:AB_2255663
phospho-TBK1 (Ser172)	Cell Signaling Technology	Cat# 5483, RRID:AB_10693472
NF-κB p65	Cell Signaling Technology	Cat#8242, RRID:AB_10859369
Phospho-NF-κB p65 (Ser536)	Cell Signaling Technology	Cat##3033
LC3	Cell Signaling Technology	Cat# 2775, RRID:AB_915950
p62	APR American Research	Cat# 03-GP62-C, RRID:AB_1542690

REAGENT or RESOURCE	SOURCE	IDENTIFIER
GAPDH	Cell Signaling Technology	Cat# 2118, RRID:AB_561053
SLC7A11	Cell Signaling Technology	Cat#98051, RRID:AB_2800296
K63-linkage Specific Polyubiquitin	Cell Signaling Technology	Cat#5621 RRID:AB_10827985
anti-actin	Sigma-Aldrich	Cat# A1978, RRID:AB_476692
goat anti-rabbit HRP secondary antibody	Agilent	Cat# P0448, RRID:AB_2617138
goat anti-mouse HRP secondary antibody	Agilent	Cat# P0447, RRID:AB_2617137
rabbit anti-guinea pig HRP-conjugated antibody	Dako	Cat# P-0141
Bacterial and virus strains		
The hypermotile AIEC strain NRG857c	Dr. Brian K. Coombes	Elhenawy et al.[39]
Chemicals, peptides, and recombinant proteins		
Murine M-CSF	PeproTech	Cat#315-02
Lipoploysaccharide(LPS)	Sigma-Aldrich	Cat#L5418
Interferon gamma (IFNγ)	BD Biosciences	Cat#554587
Liberase TL	Roche	Cat# 05401020001
Bafilomycin A1	Selleck Chemicals	Cat# S1413
MG132	Selleck Chemicals	Cat# S2619
Puromycin	InvivoGen	Cat# ant-pr-1
Alt-R® S.p. Cas9 Nuclease V3	IDT	Cat# 1081058
CpG1826	INVIVOGEN	Cat# tlrl-1826
Critical commercial assays		
TMT10 reagents	Thermo Fisher Scientific	lot# RF231770
CpG1826	INVIVOGEN	Cat# tlrl-1826
iScript™ cDNA Synthesis Kit	Bio-Rad	Cat# 1708891
SYBR Green Supermix	Bio-Rad	Cat #1725121
RNeasy Plus Mini Kit	Qiagen	Cat#74134
Glutamine Assay Kit	Abcam	Cat# ab197011
Glutamate Assay Kit	Abcam	Cat# ab83389
Glutathione Assay Kit	Thermo Fisher Scientific	Cat# EIAGSHC
Cytometric Bead Assay Flex Set	BD Biosciences	Cat#562261, Cat#562278, Cat#562336, Cat#562264, Cat#562233, Cat#562236.
Mouse IFN-beta ELISA Kit	R&D	Cat# 42400-1
Mouse CXCL1/KC DuoSet ELISA	R&D	Cat# DY453-05
Mouse CXCL2/MIP-2 DuoSet ELISA	R&D	Cat# DY452-05
P3 Primary Cell 4D-NucleofectorTM X Kit S	Lonza	Cat# V4XP-3032
Deposited data		
RNA-sequencing data	This paper	GSE206124; https://www.ncbi.nlm.nih.gov/geo/query/acc.cgi?&acc=GSE206124
Proteomic data	This paper	ftp://MSV000092110@massive.ucsd.edu/
Experimental models: Organisms/strains		

REAGENT or RESOURCE	SOURCE	IDENTIFIER
Beclin1$^{flox/flox}$-LysM-Cre^{+} mice	Herbert Virgin lab (Washington University in St. Louis)	Park et al.[8]
Beclin1$^{F121A/F121A}$ mice: B6.129(Cg)-*Becn1*$^{tm2.1Blev}$/J	Beth Levine lab (University of Texas Southwestern)	Fernandez et al. [26]
Oligonucleotides		
qRT-PCR primers, see Table S3	This paper	N/A
RNF128 sg1, GTCACAATGGTCATCGAAGT	This paper	N/A
RNF128 sg2, ATAATTACGGCAGCAACCGT	This paper	N/A
Mm.Cas9.SLC7A11.1.AA, CTCCAAAGGAGGTTACCTGC	IDT	N/A
Mm.Cas9.SLC7A11.1.AB, GATGTAGCGTCCAAATGCCA	IDT	N/A
Alt-R® CRISPR-Cas9 crRNA Negative Control#2	IDT	Cat# 1072546
Alt-R® CRISPR-Cas9 tracrRNA	IDT	Cat# 1072533
Recombinant DNA		
pXPR_BRD003 vector	Broad Institute	N/A
Software and algorithms		
Tophat2	Kim et al.[54]	https://ccb.jhu.edu/software/tophat/index.shtml
Htseq-count	Anders et al.[55]	https://htseq.readthedocs.io/en/release_0.11.1/index.html
edgeR (R package)	Robinson et al.[56]	N/A
Flowjo	FLOWJO	https://www.flowjo.com/
GraphPad Prism	GraphPad Software,Inc.	https://www.graphpad.com/